Science of The Total Environment, Volume 694, 1 December 2019, 133717

MORPHOLOGY OF ZNO NANOSTRUCTURES MODULATES THE EFFECTS OF NANO-ZNO ON BIOENERGETICS AND STRESS RESPONSE BIOMARKERS OF A MARINE BIVALVE *MYTILUS EDULIS*

Halina I. Falfushynska[1,2], Fangli Wu[1], Fei Ye[3], Nadiia Kasianchuk[2], Joydeep Dutta[3], Sergey Dobretsov[4,5], Inna M. Sokolova[1,6]

[1]Department of Marine Biology, Institute for Biological Sciences, University of Rostock, Rostock, Germany

[2]Department of Human Health, Physical Rehabilitation and Vital Activity, Ternopil V. Hnatiuk National Pedagogical University, Ternopil, Ukraine

[3]KTH Royal Institute of Technology, Material and Nanophysics Applied Physics Department, School of Science, Stockholm, Sweden

[4] Department of Marine Science and Fisheries, College of Agricultural and Marine Sciences, Sultan Qaboos University, Al Khoud 123, PO Box 34, Muscat, Oman

[5] Center of Excellence in Marine Biotechnology, Sultan Qaboos University, Al Khoud 123, PO Box 50, Muscat, Oman

[6]Department of Maritime Systems, Interdisciplinary Faculty, University of Rostock, Rostock, Germany

KEYWORDS

Nanoparticles, nanorods, ZnO, ecotoxicology, stress, Mytilus

ABSTRACT. Biofouling causes massive economical losses in maritime sector creating urgent need for effective and ecologically non-harmful antifouling materials. Zinc oxide (ZnO) nanorod coatings show promise as an antifouling material; however, their toxicity to marine organisms is not known. We studied compared toxicity of suspended and immobilized ZnO nanorods (NR) with that of ZnO nanoparticles (NP) and ionic Zn^{2+} in a marine bivalve *Mytilus edulis*. Multi-biomarker assessment included bioenergetics markers (tissue energy reserves, activity of mitochondrial electron transport system and autophagic enzymes), expression of apoptotic genes, and general stress biomarkers (oxidative lesions, lysosomal membrane stability and metallothionein expression) in the mussels. All Zn-containing exposures led to lysosomal membrane destabilization in hemocytes, but no strong disturbance of the whole-organism energy status. Exposure to NP and NR caused accumulation of oxidative lesions in proteins and lipids, stimulated autophagy, and led to overexpression of apoptosis- and inflammation-related genes. No induction of apoptotic or inflammatory pathways was seen in Zn^{2+} exposures. Unlike ionic Zn^{2+}, ZnO NP and NR share similar toxic mechanisms with strong pro-apoptotic and inflammatory signatures, but the NR toxicity is less than that of the NP at the same concentrations. Therefore, ZnO NRs have potential as low toxicity antifouling coatings in marine environments.

INTRODUCTION

Engineered nanomaterials (i.e. materials containing particles with one or more dimensions in the size range 1-100 nm) are increasingly used in industrial applications and consumer products due to their stability and novel properties compared to those of the bulk material [1]. A key feature of engineered nanomaterials, which makes them of interest to many applications, is high reactivity due to the high surface to volume ratio of nanoparticles; however, this characteristic also raises concerns about the environmental and human health hazard of nanomaterials during their production, use or release into the environment [1]. One of the important new application areas for nanomaterials is the protection of the submerged surfaces (such as ships and underwater infrastructure) from biofouling[2]. Biofouling is undesirable growth of organisms on submerged surfaces, especially prominent in marine environments [3]. Biofouling causes multi-billion dollar damage and losses to marine installations (such as ships, nets, cages, pipes, buoys) around the world. To protect submerged structures from biofouling, industries commonly use the surface coatings that contain highly toxic biocides such as copper or Irgarol [4-6]. These biocides prevent or slow down biofouling but also kill non-target organisms and accumulate in the sediments resulting in a long-term damage to marine ecosystems [4-7]. Therefore, there is an urgent need to develop effective low-toxicity alternatives to control biofouling. Nanomaterial-based coatings (including zinc oxide (ZnO) nanorods) have been recently proposed as an alternative to toxic antifouling coatings [2, 8, 9]. ZnO nanorods prevent biofouling by the production of reactive oxygen species (ROS) during photocatalysis of water [2]; due to the short life of the ROS in sea water the ZnO nanorod coatings are expected to be toxic only in the immediate vicinity of the coated surface. Furthermore, surface-supported ZnO nanocoatings have increased stability and lower release of Zn^{2+} ions compared with ZnO nanoparticles [9, 10]. Nevertheless, there remains a possibility of ZnO nanorod release into the marine environment due to the peeling or aging of the coating, making it important to investigate the possible toxic effects of these novel ZnO nanostructures on marine organisms.

The blue mussels (*Mytilus* spp.) are ecosystem engineers and common fouling organisms that form dense settlements (called mussel beds) on natural and artificial hard substrates in subtidal and intertidal zones of temperate to subarctic coastal ecosystems around the world [11, 12]. Blue mussels are common sentinel organisms used for environmental monitoring and ecosystem health assessment [13, 14]. Owing to this, their molecular and physiological responses to stress are well understood [13, 15-19] making them ideal model species for investigating the effects of novel stressors, such as new nanomaterials. Mussels are suspension feeders filtering large amounts of water through their bodies and selectively retaining particles in the size range 10-50 μm (but occasionally as small as 7 μm and as large as 80-100 μm)[20, 21]. This creates a strong potential for the uptake of nanoparticles (NPs)

and nanoparticle aggregates by the mussels and for the NPs interference with the function of the filtration organs (i.e. the gills) as well as the digestive gland of the mussels [22, 23].

ZnO nanoparticles present a toxicity risk to a broad range of aquatic organisms including microorganisms, algae, invertebrates and vertebrates [review in: [24, 25]]. ZnO nanoparticles are thought to exert toxicity through the release of zinc ions, production of reactive oxygen species (ROS) and direct particle interaction causing physical damage through internalization [26, 27], albeit studies in freshwater mussels and amphibians show different profiles of stress biomarkers induced by ZnO nanoparticles and ionic Zn^{2+} indicating different toxicity pathways of these two forms of Zn [22, 23, 28]. Most studies to date were conducted on freshwater organisms and at a relatively high, not environmentally relevant concentrations [24, 25], and the effects of ZnO nanomaterials on marine sentinel organisms such as the mussels are not well known. The available data show negative effects of ZnO nanoparticles on byssus production and adhesion capacity in *Mytilus corruscus* [29], and expression of genes encoding enzymatic antioxidants and stress kinases in *Mytilus galloprovincialis* [30]. Furthermore, most ecotoxicological studies conducted to date focus on the commercially produced spherical ZnO nanoparticles such as commonly used in cosmetics, sunscreens, and textiles [24, 25, 31]. To the best of our knowledge, no studies have focused on the toxicity of ZnO nanorods in marine organisms. Studies on human lymphocytes, hepatocellular carcinoma and endothelial cell lines [32], bacteria [33, 34], algae [35], and a freshwater crustacean *Daphnia magna* [36] report toxicity of ZnO nanorods, albeit the mechanisms of the toxic effects remain poorly understood. Notably, studies on the human cell lines showed that ZnO nanorods were more toxic to A549 cells than spherical ZnO NPs [37]. This is consistent with the notion that toxicity of nanomaterials depends on size, shape and the surface properties of the nanostructures rather than on the composition of the bulk material [38].

The aim of our present study was to investigate the toxicity of ZnO nanorods in the blue mussel *M. edulis*, and compare toxicity of immobilized and suspended ZnO nanorods to that of the better characterized ZnO nanoparticles. We tested effects of environmentally relevant (0.12 μM) and high (1.2 μM) concentrations of suspended ZnO nanoparticles and nanorods, as well as the effects of ZnO nanorods immobilized on the glass surface, on energy metabolism, general stress responses and induction of apoptosis in *M. edulis*, To assess whether nano-ZnO exposures led to a disruption of energy balance reflecting suppression of aerobic metabolic pathways and/or elevated energy costs of detoxification [39], we determined the effects of ZnO nanomaterials on activity of the mitochondrial electron transport system (ETS), tissue energy reserves (carbohydrates, lipids and proteins) and the activity of autophagic enzymes (total and free catepsin D). Activation of autophagic pathways allows recycling intracellular proteins and organelles for energy and is typically induced by cellular energy deficiency or extensive damage [40]. Induction of apoptosis by nano-ZnO was

tested by determining mRNA expression of key genes involved in regulation of the intrinsic (stress-induced) apoptotic pathway (caspases 2, 3 and 8, Bcl-2 and BAX) and cell survival (TAK1, NF-κB and inhibitors of NF-κB 1α and 2α). Oxidative stress as a potential mechanism for apoptosis induction and a general cellular stress marker, was assessed by measuring the level of oxidative lesions in proteins (carbonyls) and lipids (malondialdehyde), and general cellular stress was assessed by measuring lysosomal membrane stability in hemocytes [41]. Tissue levels of metallothioneins were measured to determine whether the toxic effects of different forms of nano-ZnO are associated with elevated tissue levels of Zn, which is a known metallothionein inducer [42]. This study provides insights into the toxic mechanisms of different forms of nano-ZnO, demonstrates distinct biomarker profiles of nano-ZnO compared with ionic Zn^{2+} and shows that ZnO nanorods are less toxic than conventional ZnO nanoparticles at comparable sublethal concentrations, yet more toxic than dissolved Zn^{2+}.

MATERIALS AND METHODS

Preparation and characterization of ZnO nanostructures. Attached (NRA) or suspended (NR) ZnO nanorods were prepared using a two-step process described elsewhere {Al-Fori, 2014 #16746 Briefly, a seed layer of ZnO nanocrystallites was deposited on surfaces of cleaned microscope glass slides (size 75 × 25 mm) and used to grow NRs. The samples were annealed in an atmospheric furnace at 350°C for 5 h and stored in an oven at 95 °C until further use. This resulted in homogenious growth of nanorods with the length of >500 nm and the diameter of about 80 nm. The average amount of ZnO nanorods was estimated by using a QC microbalance attached to Thermo gravimetric analysis (TGA) (PerkinElmer Frontier 1, USA) and found to be 0.2655 ± 0.0259 mg/cm^2. To prepare suspension of ZnO nanorods (NR), immobilized ZnO NR (NRA) were scraped with sterile scalpel and suspended in seawater to reach desired concentrations. Commercial ZnO nanoparticles (NPs) (manufacturer's reported average size 30 nm) were purchased from Sigma-Aldrich (Taufkirchen, Germany). The morphology of NPs and synthesized immobilized or suspended NRs were characterized using filed-emission scanning electron microscopy (FE-SEM, GEMINI® Ultra 55, Carl Zeiss AB, Sweden). High resolution transmission electron microscopy (HR-TEM, JEM-2100F, JEOL (Nordic) AB, Sweden) was employed to examine the morphology and crystal structure of ZnO nanoparticles and free-standing ZnO nanorods. The concentration of zinc in ZnO samples was measured by inductively coupled plasma atomic emission spectroscopy (ICP-AES, iCAP 6500 ICP Spectrometer, Thermo Scientific Inc., U.S.). Suspension of ZnO nanoparticles and nanorods was prepared in salinity 15 water (NaCl equivalent), and the size distribution was measured using the particle size analyzer (Delsa™ Nano C, Beckman Coulter Inc., USA).

Animal collection and exposures. Mussels were collected near Warnemünde, Germany (54°10´49.602"N, 12°05´21.991"E). All Baltic populations of *Mytilus* represent *Mytilus edulis*

× *M. trossulus* hybrids, and the studied *Mytilus* population has ~70% and 100% of the nuclear and mitochondrial genetic background, respectively, that identifies with *M. edulis* [43]. Based on the predominance of *M. edulis* genes in the studied natural hybrids, we designated experimental animals as *M. edulis*. The mussels were transported in sea water to the University of Rostock within 2 h of collection. The shells were cleaned from epibionts, and the mussels were kept in aerated, temperature-controlled recirculated aquaria with a multi-step filtration system including UV-water treatment, protein skimmer and a moving bed biofilter. Mussels were acclimated at 15±1°C and salinity 15±1 for at least four weeks prior to the experiments. Average shell length of experimental mussels was 45.4±0.7 mm, soft body mass 4.32±0.21 g (N=24).

After the preliminary acclimation, mussels were randomly assigned to one of the following eight groups: 1) control (no Zn addition); 2) 0.12 µM Zn as ZnO nanoparticles (NP-L); 3) 1.2 µM Zn as ZnO nanoparticles (NP-H); 4) 0.12 µM of Zn as suspended ZnO nanorods (NR-L); 5) 1.2 µM of Zn as suspended ZnO nanorods (NR-H); 6) adherent ZnO nanorods (NRA) on a glass slide; 7) 0.12 µM of Zn^{2+} as $ZnSO_4$ (Zn-L); 8) 1.2 µM of Zn^{2+} as $ZnSO_4$ (Zn-H). Each group was randomly subdivided and placed into 2-3 replicate tanks, each tank containing 15 mussels in 5 L of artificial seawater (ASW) (Instant Ocean, Aquarum Systems, Sarrebourg, France). For nano-ZnO and ionic Zn exposures, a static renewal design was used with water change and Zn addition twice a week. Following the water change, 10,000-fold concentrated NP or NR suspensions, or $ZnSO_4$ solution in ultrapure water was added to the respective experimental tanks to achieve a nominal concentration of 0.12 µM (10.0 µg L^{-1}) or 1.23 µM (100.0 µg L^{-1}) Zn. For immobilized ZnO NR exposures, one glass slide (19.5 cm^2 each, concentration of ZnO = 1.035 mg/L; 12.3 µM) was placed into each replicate tank covering XX% of the bottom surface. The rational of using such high ZnO concentrations was to mimic the potential effect ZnO nanorod coatings on mussels attaching to surfaces coated with ZnO nanorods. In our experiment, mussels predominantly attached to the slides with immobilized ZnO. Ionic Zn treatments were to test whether the observed effects of nano-ZnO can be ascribed to the release of Zn^{2+}. Control mussels (C) were maintained under the same conditions but without addition of ZnO nanomaterials or Zn^{2+}. Mussels were exposed for 14 days to different conditions in 12:12 light: dark period. The OSRAM L58W7840 Lumilux T8 (color temperature 4000 K) lamps were used as a light source. The light intensity measured in the experimental tanks during the light period was 2.69±0.18 µmol photons s^{-1} m^{-2} (N=4). All exposures were conducted at 15±1°C and salinity 15±1. During preliminary acclimation and experimental exposures, mussels were fed *ad libitum* on alternate days with a commercial blend of live algae containing *Nannochloropsis oculata, Phaeodactylum* sp. and *Chlorella* sp. (Premium Reef Blend, CoralSands, Wiesbaden, Germany) per manufacturer's instructions. No mortality of the mussels occurred during the experimental exposures except of NRA group where 12% of mussels died after 14 days.

After 14 days of experimental exposure, mussels were dissected on ice, and blood (hemolymph) and soft tissues were collected. Lysosomal membrane stability was determined in hemocytes, all other traits (oxidative stress indices, enzyme activities, metallothionein concentration, energy reserves, ETS activity and mRNA expression of target genes) were evaluated in the whole soft tissue. Hemocytes were studied immediately after sampling, while whole soft tissue samples were shock-frozen in liquid nitrogen and stored at –80°C until further analyses. No effects of experimental tanks on the studied traits were found in a pilot analysis ($P>0.05$), and individual mussels were used as biological replicates.

Oxidative stress markers. Lipid peroxidation (LPO) was determined in the total soft tissue homogenate (1:10 w:v) by the production of TBA-reactive substances (TBARS) [44]. The absorbance of the chromogen was determined at 532 nm using a SpectraMax M2 microplate reader (Molecular Devices GmbH, Biberach-an-der-Riß, Germany) with the LightPath correction. A molar extinction coefficient of $1.56 \cdot 10^5$ $M^{-1} \cdot cm^{-1}$ was used.

Protein carbonyl (PC) concentration, as index of protein oxidation, was measured in the trichloroacetic acid-treated total soft tissue homogenate (1:10 w:v) samples by the reaction with 2,4-dinitrophenylhydrazine (DNPH)[45]. Differences in the absorbance between the DNPH- and the HCl-treated samples were determined spectrophotometrically at 370 nm using a SpectraMax M2 microplate reader (Molecular Devices GmbH, Biberach-an-der-Riß, Germany) with the LightPath correction, and the amount of carbonyls was determined by using molar extinction coefficient of $2.2 \cdot 10^4$ $M^{-1} \cdot cm^{-1}$. Data were expressed as μmol $PC \cdot g^{-1}$ FW.

Quantification of metallothioneins (MTs). Metallothioneins (MTs) were determined in total soft tissue according to a published protocol [46] after ethanol/chloroform extraction with DTNB and calculated by assuming the relationship: 1 mol MT-SH = 20 mol GSH and expressed as μg of MTs per gram of wet mass.

Cathepsin D activity. Cathepsin D (EC 3.4.23.5) activity was determined in the whole soft tissue homogenate in 0.25 M sucrose (1:2 w: v) with 1% hemoglobin as substrate [47]. Cathepsin D has effect on acid denatured hemoglobin resulting in a soluble colored complex which can be read spectrophotometrically at 280 nm using a SpectraMax M2 microplate reader (Molecular Devices GmbH, Biberach-an-der-Riß, Germany) with the LightPath correction. Free cathepsin D activity was assessed in total soft tissue homogenate without detergent addition, whereas the total cathepsin D activity was measured after the enzyme release by Triton X100 treatment. Lysosomal cathepsin D activity was calculated as a difference of total and free activities. Activities were determined using a standard curve with tyrosine, and expressed as nmol tyrosine min^{-1} mg^{-1} of soluble extracted protein.

Energy reserves. Energy reserves (lipids, proteins and carbohydrates) were assessed in the gill and the whole tissue of *M. edulis*. Lipid content was measured using chloroform-methanol method [48]. Approximately 50 mg of tissue powder was added to 3 mL of chloroform: methanol mixture (1:1, v: v), incubated for 5 min with vigorous mixing, and centrifuged at 3,000 x *g* for 4 min to remove the debris. Extracted lipids or soybean oil standards (250 µL per sample) were dried out at 100°C for ~10-12 min. 100 µL of 98% sulfuric acid (H_2SO_4) was added to each sample and heated at 100°C for 10 min. The sample was cooled down to room temperature, mixed with 2.4 mL of vanillin reagent (600 mg vanillin in 100 mL of hot water mixed with 400 mL of 85% phosphoric acid) and incubated for 5 min.

For determination of the carbohydrate and soluble protein content, ~50 mg of tissue powder was mixed with ultrapure water containing 0.1% Triton (1:10 tissue mass to volume). Cells were lysed by three rapid freeze-thaw cycles at -80°C and centrifuged at 3,000 x *g* for 3 min to remove the debris. Carbohydrate concentrations were measured using phenol-sulfuric acid method [49]. Samples or glucose standards (200 µL) were mixed with 600 µL of concentrated H_2SO_4, immediately followed by addition of 120 µL of 5% phenol. Samples were incubated for 5 min at 90°C, cooled and used to determine the carbohydrate content. Protein concentrations were measured using Biorad Bradford Protein Assay Kit according to the manufacturer's instructions (Bio-Rad, Hercules, CA, USA) with BSA as a standard. The absorbance was read at 490, 492 and 595 nm for lipids, carbohydrates and proteins, respectively, using a SpectraMax M2 microplate reader (Molecular Devices GmbH, Biberach-an-der-Riß, Germany). Total energy reserve was calculated using energy equivalents of 39.5 kJ g^{-1}, 17.5 kJ g^{-1} and 24 kJ g^{-1} for lipids, carbohydrates, and proteins, respectively [50].

Activity of mitochondrial electron transport system (ETS) and non-mitochondrial reductases. ETS activity was measured in the whole-body extracts of *M. edulis* using (2-(4-iodophenyl)-3-(4-nitrophenyl)-5-phenyl tetrazolium chloride) (INT) tetrazolium reduction assay as described elsewhere [51, 52]. Briefly, whole body of mussels was homogenized with ETS-B solution (153 µM $MgSO_4$, 1.5 mg ml^{-1}polyvinylpyrrolidone, and 0.2% (v: v) Triton X-100 in 0.1 M Tris-HCl, pH 8.5) at 1:50 (w: v) ratio. The homogenate was centrifuged at 3000 x *g* for 10 min at 4°C, and supernatant used to assess the ETS activity as the rate of the NAD(P)H-dependent reduction of INT-tetrazolium to formazan at 20°C[52]. The potential non-mitochondrial reduction of INT-tetrazolium in the samples was determined by addition of 10 µM of rotenone and 675 mM of KCN (inhibitors of the mitochondrial Complex I and IV, respectively) to the assay. ETS activity was calculated by subtracting the blank slopes from the reaction slopes for each sample. Specific ETS activity of the tissues (µmol O_2 min^{-1} mg wet tissue mass) was calculated from the rotenone- and KCN-sensitive rate of INT reduction using the extinction coefficient of formazan of 15.9 mM^{-1} cm^{-1} and the stoichiometric equivalent of 1 µmole formazan to 0.5 µmole O_2, and expressed as nmole O min^{-1} g^{-1} wet body

mass. The activity of non-mitochondrial reductases was calculated from the rotenone- and KCN-insensitive rate of INT reduction and expressed mU g^{-1} wet body mass.

Quantitative RT-PCR. Total RNA was extracted from the whole tissue samples of control and nano-ZnO-exposed mussels using TRI reagent (Sigma, St. Louis, MO) according to the manufacturer's protocol. Tissue to TRI reagent ratio was kept below 1:10 (w: v). this method yielded high purity total RNA with 280/260 absorbance ratio > 1.9. RNA samples were cleaned up from possible DNA contamination using TURBO DNA-free Kit (Thermo Fisher Scientific, Berlin, Germany) was used according to the manufacturer's instructions. cDNA was obtained from 2 µg of total RNA using High Capacity cDNA Reverse Transcription Kit (Thermo Fisher Scientific, Berlin, Germany) according to the manufacturer's instructions. Quantitative PCR was carried out using StepOnePlus™ Real-Time PCR System Thermal Cycling Block (Applied Biosystems, Thermo Fisher Scientific, Berlin, Germany) and Biozym Blue S'Green qPCR Mix Separate ROX kit (Biozym Scientific GmbH,_Hessisch Oldendorf, Germany) according to the manufacturer's instructions. Reaction mixture containing 10 µL of 2x qPCR S'Green BlueMix and ROX additive mixture, 1.6 µL of each forward and reverse primer (to the final concentration of 0.4 µmol L^{-1}), 4.8 µL PCR grade water and 2 µL of cDNA sample were added to the wells of 96 well PCR plates, sealed (RT-PCR Seal foil, Roth, Karlsruhe, Germany) and briefly centrifuged to collect the contents and eliminate air bubbles. The cycling parameters were as follows: 95°C for 10 min to activate the polymerase followed by 40 cycles of 15 s at 95°C and 60 s at 60°C. Following the amplification, a melt curve analysis was performed to ensure that only a single PCR product was amplified. Two replicates were done for each sample. In each run, serial dilutions of a cDNA standard were amplified to determine amplification efficiency [53]. The apparent amplification efficiency was calculated, and the expression of the target genes was normalized against the expression of a housekeeping gene as described elsewhere [53, 54]. In a pilot study, three housekeeping genes (β-actin, tubulin and eukaryotic elongation factor eEF1) were tested, and the least variable eEF1 was used as a housekeeping gene for normalization of the target genes [caspase 2, caspase 3, caspase 8, Bcl2, BAX, TGF-β-activated kinase 1 (TAK1), nuclear factor kappa B-1 (NF-κB1), inhibitor of nuclear factor kappa B-1 (IKK1) and inhibitor of nuclear factor kappa B-2 (IKK2)].

General stress markers. Hemolymph was withdrawn from the adductor muscle sinus. Hemocytes were washed and pelleted at 500 × *g* using a hemocyte (HC) buffer containing 20 mmol L^{-1} Hepes, 436 mmol L^{-1} NaCl, 53 mmol L^{-1} $MgSO_4$, 10 mmol L^{-1} $CaCl_2$ and 10 mmol L^{-1} KCl, pH 7.3. Hemocytes were enumerated using BrightLine hemacytometer. Hemocytes resuspended in HC buffer, diluted to 1×10^7 cells/mL, then aliquoted for analyses. Lysosomal membrane stability was determined in hemocyte suspension by the Neutral Red Retention (NRR) assay as described elsewhere [55].

Statistics. Data were tested for the normality and homogeneity of variances using Kolmogorov-Smirnov and Levine test, respectively. For the data deviating from normality or homogeneity of variances, Box-Cox or $\log_{10}$ transformation was used. If the transformations did not result in normal distribution, non-parametric Wilcoxon-Mann-Whitney test was used. The effects of nano-ZnO exposure on the biological traits were tested using one-way ANOVA. Normalized, Box-Cox transformed data were subjected to the principal component analysis (PCA) to reduce the dimensionality of the data set and identify the potential biomarker signatures of different experimental exposures. The classification tree based on all studied trait was built using Classification and Regression Tree (CART) software using raw (non-transformed) data.

The integrated biomarker response (IBR) indexes were calculated using CALculate IBR Interface (Calibri, https://liec-univ-lorraine.shinyapps.io/calibri/) as described elsewhere [56]. IBR was calculated and IBR radar plots generated separately for mRNA expression of target genes, and for stress and toxicity biomarkers because Calibri interface allows uploading a maximum of seven traits.

All statistical calculations except IBR were performed with Statistica v. 12.0 and Excel for Windows-2013. Differences were considered significant if the probability of Type I error was less than 0.05.

RESULTS

Nanomaterials characterization. The average particle size of commercial ZnO nanoparticles (NPs) was 30.1±6.3 nm (mean ± S.D., N = 200). TEM images of NPs at higher magnification show two lattice spacings of 2.45 Å and 2.60 Å corresponding to (101) and (002) lattice planes of zinc oxide, respectively (**Fig. 1 II, III**). Figure 1 Ic shows the selected-area electron diffraction (SAED) pattern of ZnO nanoparticles. Several diffracted spots on different rings were selected to calculate the lattice spacing in real space. The first three ring patterns with strong intensity represent (100), (002) and (101) planes of ZnO wurtzite structure. Diffraction patterns of ZnO from other lattice planes of (102), (110), (103), (200), (112) and (201) are found.

ZnO nanorods (NRs) (**Fig. 1 II**) had length from a few hundreds to a thousand nanometers and the lattice spacing of 2.60 Å corresponding to the distance between (002) crystal planes, which indicates [001] as the growth direction for NRs (**Fig. 1 IIb**). The SAED image of a ZnO nanorod shows the single crystalline nature of NRs (**Fig. 1 IIc**). Immobilized ZnO nanorods (NRA) have the same structure as suspended NRs (**Fig. 1**). The size distribution of NPs in water was in a similar range for two different particle concentrations with a peak of size distribution ~ 100 nm (**Supplementary Fig. 1**). Suspended NRs have size distribution in a range from 200 nm to 1 μm.

Oxidative stress markers. Exposure to ZnO NPs (0.12 and 1.2 μM) led to accumulation of oxidative lesions to lipids and proteins in *M. edulis* as indicated by elevated levels of TBARS and/or carbonyl groups in proteins (**Fig. 2A, B**). Exposure to high concentration (1.2 μM) of ZnO NRs and 0.12 μM Zn^{2+} also led to accumulation of TBARS and protein carbonyls (**Fig. 2A, B**). Attached ZnO nanorods, 0.12 μM of suspended ZnO NRs or 1.2 μM Zn^{2+} had no effect on the studied oxidative markers (**Fig. 2**).

Metallothioneins. Concentrations of metallothioneins were significantly upregulated in the mussels exposed to 0.12 μM ZnO NPs, 1.2 μM ZnO NRs, and 0.12 μM Zn^{2+} (**Fig. 2C**). In all other treatments, no increase in MT concentrations was found in the mussels' body.

Lysosomal membrane stability. Lysosomal membrane stability measured by the ability of the cell to take up and retaina vital dye Neutral Red was significantly suppressed in hemocytes of *M. edulis* exposed to 0.12 and 1.2 μM ZnO NPs, 1.2 μM ZnO NRs, and 0.12 μM Zn^{2+} (**Fig. 2D**). No significant decline in the lysosomal membrane stability was found in the hemocytes of mussels exposed to 0.12 μM ZnO NRs, attached nanorods, or 1.2 μM Zn^{2+} (**Fig. 2D**).

Autophagic markers. Exposure to 0.12 μM ZnO NPs, 1.2 μM ZnO NRs, and 0.12 μM Zn^{2+} stimulated the total cathepsin D activity as well as release of free cathepsin D in the mussels (**Fig. 2E, F**). All other treatments had no significant effects on the total or free cathepsin activity.

Energy reserves. Low concentrations (0.12 μM) of ZnO NPs and NRs led to a significant decline of body lipid content of *M. edulis* (**Fig. 3A**). Low concentrations (0.12 μM) of ZnO NPs and dissolved Zn^{2+} led to elevated concentrations of carbohydrates (**Fig. 3B**). All other treatments had no significant effect on the body lipid or carbohydrate content (**Fig. 3A, B**). Protein content of *M. edulis* was not affected by experimental exposures to nano-ZnO or dissolved Zn^{2+} (**Fig. 3C**). Exposure to 0.12 μM ZnO NPs (but none of the other experimental exposures) resulted in a significant decline of the total energy reserve of the *M. edulis* bodies (**Fig. 3D**).

ETS and non-mitochondrial reductases. Whole-body ETS activity of the mussels was suppressed by exposures to 1.2 μM ZnO NPs, 0.12 μM ZnO NRs and attached ZnO NRA (**Fig. 4A**). Exposure to ionic Zn^{2+}, 0.12 μM ZnO NPs, or 1.2 μM ZnO NRs had no effect on the ETS activity (Fig. 4A). Activity of non-mitochondrial reductases was stimulated by 1.2 μM ZnO NPs, 0.12 and 1.2 μM ZnO NRs, and NRA (**Fig. 4B**). Exposure to ionic Zn^{2+} had no effect on the activity on mitochondrial reductases (**Fig. 4B**).

Apoptotic markers. Exposure of mussels to suspended ZnO NPs led to a concentration-dependent increase in mRNA expression of caspase 2, caspase 3, TAK1, NF-κB and Bcl-2 (**Fig. 5**). Caspase 2 mRNA was upregulated by ~8 and ~270-fold in the mussels exposed to 0.12

and 1.2 μM ZnO NPs, respectively (**Fig. 5A**). Caspase 3 mRNA levels were upregulated by ~5-fold by exposure to 1.2 μM (but not to 0.12 μM) ZnO NPs (**Fig. 5B**). Expression of TAK1 and NF-κB mRNA increased by ~4-6-fold at 0.12 μM ZnO NPs and by ~10-15-fold at 1.2 μM ZnO NPs exposures (**Fig. 5D, E**). Levels of Bcl-2 mRNA increased by ~4 and 6-fold in the mussels exposed to 0.12 and 1.2 μM ZnO NPs, respectively (**Fig. 5F**). mRNA expression of caspase 8, BAX, IKK1 and IKK2 were not affected by exposure to ZnO NP (**Fig. 5C, G, H, I**).

Exposure to suspended ZnO nanorods (NRs) upregulated mRNA expression of apoptotic markers in the mussels similar to the effects of ZnO NPs, albeit the stimulatory effects of ZnO NRs on apoptotic markers were generally lower than at the respective concentrations of NPs. Thus, exposure to a low concentration (0.12 μM) of ZnO NRs upregulated mRNA levels of caspase 2 and 3 by ~4-6-fold, and those of TAK1, Bcl-2 and IKK2 by ~2-fold (**Fig. 5A, B, D, F, I**). Exposure to 1.2 μM ZnO NRs upregulated mRNA levels of caspase 3, TAK1, NF-κB and Bcl-2 by ~40, 12, 10 and 5-fold, respectively (**Fig. 5A, D, E, F**). mRNA expression of caspase 8, BAX and IKK1 was not affected by exposure to ZnO NRs (**Fig. 5C, G, H**).

Exposure to attached ZnO nanorods stimulated mRNA expression of caspase 2 (by ~420-fold), TGF-β, NF-κB (by ~10-fold) and Bcl-2 (by ~2-fold) in *M. edulis*. Exposure to the waterborne soluble Zn^{2+} had no stimulatory effect on mRNA expression of the studied apoptotic markers (**Fig. 5**).

Data integration. Principal component analysis (PCA) using all studied bioenergetics and stress-related traits identified three principal components (PC) jointly explaining 57% of variation of the data (**Supplementary Table 1**). The 1st PC explaining 20.4% of variance had high positive loadings (>0.5) of free cathepsin D and ETS activities and high negative loadings (<-0.5) of caspases 2, 3 and 8, Bcl2, TGF-β, NF-κB and CEA (**Supplementary Table 1; Fig. 6**). The 2nd PC (explaining 16.6% of variance) had high positive loadings of TBARS, total and free cathepsin D activity, Bcl2, TGF-β, NF-κB and high negative loadings of the lysosomal membrane stability marker (NRR) (**Supplementary Table 1; Fig. 6**). The 3rd PC (12.6% of variance) had high positive loadings of inhibitor of NF-κB 2α mRNA levels, and of body concentrations of carbohydrates and proteins (**Supplementary Table 1**). The mussels exposed to low concentrations of NRs (0.12 μM Zn) group together with the control mussels and those exposed to high (1.23 μM) levels of ionic Zn in the plane of two 1st principal components (**Fig. 6**). Similarly, mussels exposed to high levels of NRs group with those exposed to low levels of NPs, and the mussels exposed to attached nanorods (NRA) group with those exposed to high levels of suspended NPs (**Fig. 6**).

IBR radar plots based on the bioenergetics markers show considerable changes in the biomarker response profiles but no consistent trend associated with exposures to ZnO NPs, NRs or ionic Zn (**Fig. 7**). IBR analysis based on general stress markers (oxidative stress markers, lysosomal membrane stability and metallothionein levels) showed similarities

between the control group and that exposed to high levels of ionic Zn (**Fig. 8**). Other groups showed increase in the general stress-related markers but no consistent pattern differences between ZnO and low Zn^{2+} exposures (**Fig. 8**). IBR radar plots based on apoptotic markers indicated similarity between the control group, and the mussels exposed to the high and low concentrations of ionic Zn, as well as the low concentration of ZnO NPs (**Fig. 9**). These groups showed low response for all studied apoptotic markers. The mussels exposed to low levels of ZnO NRs showed high response of caspases 3 and 8, but no response for other studied apoptotic markers (**Fig. 9**). In contrast, mussels exposed to high levels of NPs or NRs, and attached nanorods (NRA) showed a strong profile of apoptosis activation, which was especially pronounced in mussels exposed to the high levels of ZnO NPs (**Fig. 9**).

CART analysis showed that of all the studied traits, apoptosis markers had the most power to distinguish among the experimental treatment groups (**Fig. 10**). Thus, mussels exposed to the high concentration of NRs, attached NRs or the high concentration of NPs were separated from all other groups based on the elevated expression (>130) of caspase 2 mRNA. Of the former groups, mussels exposed to attached NRs were distinguished from those exposed to the high concentration of suspended NR based on extremely high (>814) levels of caspase 2 mRNA (**Fig. 10**). Caspase 8 was the key trait distinguishing the groups exposed to the high concentration of NPs and high concentration of NRs, with the higher caspase 8 expression in the former group. Groups exposed to ionic Zn were distinguished by low levels of caspase 2 mRNA, below those of the control group (**Fig. 10**). The lowest level of caspase 2 expression (<1.3) was characteristic of the mussels exposed to the low concentration of Zn^{2+}. Mussels exposed to the low concentration of ZnO NPs were distinguished from the control group and from the mussels exposed to the low concentration of ZnO NRs based on their low body lipid content, and the lower levels of NF-κB 2α inhibitor mRNA, respectively (**Fig. 10**).

DISCUSSION

Introduction of new nanomaterials in the marine environment (such as nano-ZnO-based antifouling coatings) carries potential risks to non-target marine organisms due to the possible release of trace metals and direct toxic effects of nanostructures. Our study showed that ZnO nanorods, a promising antifouling material (2; cite here Sathe et al.), induces toxicity and cellular stress response in a sentinel bivalve, the blue mussel *M. edulis*. The toxicity of ZnO adherent and suspended nanorods was, however, lower than that of commercially produced spheroid ZnO nanoparticles, such as commonly used in textiles and personal care products (including sunscreens). Despite different toxicity levels, ZnO nanoparticles and nanorods share similar toxicity mechanisms that are distinct from those of ionic zinc. Our data show that Zn-containing nanostructures are potentially harmful to marine organisms and their toxicity is not due to the release of free Zn^{2+} from ZnO nanostructures in seawater.

Effects of ZnO nanostructures and ionic Zn^{2+} on mussels' bioenergetics

Environmental pollutants (including trace metals) can cause energetic stress in marine organisms due to the elevated costs of detoxification, stress protection and damage repair [57]. *De novo* synthesis of proteins involved in detoxification (e.g. metallothioneins, membrane efflux pumps, or xenobiotic biotransformation enzymes) and stress protection (e.g. molecular chaperones and antioxidants) are energetically costly [39, 58, 59]. Furthermore, inflammation caused by metals or metal-containing nanostructures [37, 60, 61] may contribute to the elevated energy costs of basal maintenance [62]. Therefore, elevated energy demand for cellular homeostasis in pollutant-exposed organisms might outstrip the organism's ability to assimilate energy from the environment resulting in the mobilization of the body energy reserves such as carbohydrates (glycogen) and lipids.

Glycogen is a key energy storage compound in marine bivalves providing rapidly mobilizable substrate to support high energy flux (e.g. during reproduction or activity) or to fuel energy metabolism when other energy fuels cannot be used (e.g. during environmental anaerobiosis when the absence of oxygen prevents aerobic oxidation of lipids). Exposure to trace metals (such as cadmium, copper and zinc) as well as organic pollutants commonly results in mobilization and eventually depletion of the glycogen reserves in aquatic organisms reflecting elevated energy demand [15, 63-67]. ZnO nanoparticles can also directly affect glycogen metabolism REFERENCE?. In human hepatocytes, high exposures to ZnO (>10 μg cm^{-2} cell culture surface) stimulate both glycolysis and gluconeogenesis [68]. Carbohydrate degradation was also stimulated by ZnO NPs in bacteria *Staphylococcus aureus* [69]. Glycogen depletion was also found in freshwater bivalves *Unio tumidus* exposed to ZnO NPs (3.1 μM Zn) [22]. Our study shows that the carbohydrate stores (that consist by >90% of glycogen in mussels) are not depleted during exposure to the studied concentrations of ZnO nanostructures or ionic Zn^{2+} (corresponding to 0.12 or 1.2 μM Zn) in *Mytilus*. In fact, in two experimental groups of mussels (exposed to 0.12 μM of ZnO NPs and Zn^{2+}) the body carbohydrates content increased. This increase was associated with a strong reduction in the lipid levels in the mussels exposed to 0.12 μM ZnO NPs indicating a shift in the relative rates of lipid and glycogen synthesis and breakdown. The resulting change in the body composition led to an overall decrease in the body energy content of 0.12 μM ZnO NPs-exposed mussels. Notably, the body protein content of the mussels remained stable during the experimental exposures. This is consistent with the generally accepted role of the proteins as the last-resort energy reserve that is used during extreme energy deficiency (such as starvation) or short-term extreme energy demand such as exhaustive exercise [70, 71]. Generally, exposure to ZnO nanostructures and ionic Zn^{2+} led to a decrease in the total body energy content of experimental mussels. An opposite trend was detected for the low Zn^{2+} concentration which stimulated the glycogen build up and increased the total energy content of the mussels' bodies. However, except for the mussels exposed to low ZnO NP

concentrations, this decrease in the energy content was not significant in other experimental exposures indicating that exposure to ZnO nanostructures and ionic Zn^{2+} does not result in severe energy deficiency in *Mytilus*.

Bioenergetics stress might be exacerbated by the negative effects of ZnO nanomaterials on mitochondria that generate over 90% of cellular ATP in aerobic organisms. Trace metals, such as Zn, Cd and Cu, have direct negative impacts on mitochondrial function resulting in the suppression of the ATP synthesis capacity and a decrease in the mitochondrial efficiency [72-76]. Mitochondria are sensitive to ZnO NPs; studies in model organisms and mammalian cell lines show that long-term exposure to ZnO lead to the loss of mitochondrial membrane potential and decrease in mitochondrial activity [37, 68]. Similarly, exposure to high concentrations of ZnO (4 mg L^{-1} corresponding to 49.2 μM Zn) damaged mitochondria of a marine bivalve *Crassostrea gigas* resulting in membrane rupture, mitochondrial swelling and loss of the mitochondrial cristae [77]. Our study shows that low, environmentally relevant ZnO exposures (0.12-1.2 μM) also suppress the mitochondrial ETS activity of Mytilus albeit this effect is not consistent across all nano-Zn exposures and found only in 0.12 μM ZnO NPs, 1.2 μM ZnO NRs and ZnO NRA. It is worth noting that in our study, the total ETS capacity was assessed in the whole-body homogenates, so that the observed decline in mitochondrial ETS activity may reflect a decrease in the mitochondrial quality as well as quantity of the mitochondria in the tissue. Future studies using isolated mitochondria as well as the assessments of the mitochondrial density in different tissues are needed to resolve this question. Regardless of the underlying mechanisms, a decrease in the mitochondrial ETS capacity indicates negative impacts of nano-ZnO on bioenergetics of *Mytilus*, since ETS capacity tightly correlates with the maximum capacity for ATP synthesis in marine bivalves [15, 52, 78]. Notably, unlike nano-ZnO, exposures to ionic Zn had no negative effect on the studied bioenergetics traits of *Mytilus* indicating that the observed disturbances of energy homeostasis in ZnO-exposed mussels are unlikely to be due to the release of Zn^{2+} from the nanomaterials.

Oxidative stress in mussels to nano-ZnO and ionic Zn^{2+}

Oxidative stress has been proposed as a major toxicity mechanism for ZnO nanoparticles [26, 37] and is the putative mode of antifouling action of ZnO nanorods [2, 8]. Therefore, we anticipated that exposure of the mussels to ZnO nanomaterials would result in oxidative injury due to the elevated production of reactive oxygen species, and that this response will be stronger than in case of ionic Zn^{2+}, which is a redox inactive metal [79]. However, our data showed a modest oxidative stress response to ZnO nanostructures in Mytilus, as assessed by the indices of the lipid and protein damage, TBARS and carbonyls, respectively. This can be explained by low visible ligt intensity used during this study. The observed increase in TBARS and carbonyl content of the mussels' body was similar or lower than during

exposures to ionic Zn^{2+} and not concentration-dependent. Thus, elevated levels of TBARS indicative of the lipid damage were found in the mussels exposed to low concentrations of ZnO NPs and ionic Zn^{2+}, as well as those exposed to high concentration of ZnO NRs, but not in high Zn^{2+}, high NPs, or attached NRs exposures. Similarly, elevated levels of protein carbonyls were found in mussels exposed to high concentrations of NPs and NRs, and low concentrations of Zn^{2+}, but not in other exposures. These findings indicate that oxidative injury is not a major mechanism on nano-Zn-induced toxicity in *Mytilus* in the environmentally relevant concentration range (0.12-1.23 μM). Notably, exposures to ZnO NPs and ionic Zn^{2+} upregulated mRNA expression of antioxidant enzymes including glutathione-S-transferase, catalase and superoxide dismutase in a related mussel species, *Mytilus galloprovincialis* [30], and increased enzymatic activity of catalase and superoxide dismutase in the carpet clam *Ruditapes philippinarum* [80]. Similar to our present study, there was no indication of oxidative injury to lipids or proteins in *R. philippinarum* after prolonged (7 days) exposure to ZnO NPs corresponding to 0.012 and 0.12 μM Zn [80]. Zn^{2+} has well known antioxidant properties both at normal and supraphysiological concentrations [81], which might explain the stimulatory effects of ionic Zn (and possibly, of ZnO nanomaterials, assuming some Zn^{2+} is released) on the antioxidant defense system of mussels and clams. It is worth noting that the metallothioneins (MTs) content was significantly increased only in the mussels from the highest tested Zn exposures including high concentrations of NPs, attached NRs and high concentration of ionic Zn^{2+}. It is highky likely that the modest extent of MTs induction indicates a small increase in the intracellular Zn^{2+} burdens of experimental mussels. The main function of thiol-rich MTs is chelation of intracellular trace metals (such as Zn^{2+}, Cd^{2+} or Cu^{2+}) [82, 83] but they can also act as free radical scavengers [84, 85] so that elevated MTs levels in the mussels in high Zn exposures may contribute to increased antioxidant capacity. Therefore, taken together, our findings and the earlier published research [30, 80] show that antioxidant systems of marine bivalves are sufficient to counteract an increase in ROS production (if any) that might be caused by ZnO nanomaterials.

Lysosomal responses to Zn-containing exposures in mussels

Lysosomal membrane stability of hemocytes is commonly used as a marker of general stress response in bivalves [86, 87]. Given that lysosomes are a key intracellular target of ZnO nanoparticles [26, 37] as well as an important site of metal detoxification [88, 89], exposures to high levels of nano-ZnO are expected to result in lysosomal stress and destabilize the lysosomal membrane as was shown earlier in freshwater bivalves [22, 23, 90]. Our present study shows that a similar decrease in the lysosomal membrane stability in Mytilus exposed to ZnO NP.; However, during exposure to ZnO nanorods, only the highest concentration of suspended NRs led to destabilization of the lysosomal membrane of hemocytes shown by a decrease in NRR. This suggests that ZnO particle morphology plays a role in the lysosomal

toxicity, with the larger nanorods being generally less toxic than the smaller spheroid nanoparticles.

Exposure to ZnO NPs (0.12 μM), low levels (0.12 μM) of ionic Zn and high concentration (1.2 μM) of suspended NRs led to a slight but significant increase in the total levels of cathepsin D and a notable increase in the free cathepsin D levels. The increase in free cathepsin D was associated with a decline in the lysosomal membrane stability (measured in hemocytes as a key cell type integrating the organismal stress [91, 92]) in the mussels from the same exposure groups, consistent with the cathepsin D release from lysosomes. Activation of autophagic enzymes, such as cathepsin D, in mussels might indicate elevated recycling of intracellular structures to augment energy supply [70] and/or their increased breakdown to minimize stress-induced cellular damage [40, 93]. The former explanation appears less likely as the bioenergetics markers do not indicate energy deficiency in Zn-exposed mussels. Thus, activation of the lysosome-based quality control mechanisms to remove damaged proteins or organelles appear the most plausible explanation of the observed increase in the cathepsin D total and free activity in Zn-exposed mussels.

Modulation of cell survival pathways by exposure to ZnO nanostructures

ZnO nanostructures induce apoptotic pathways in the mussels *Mytilus,* with ZnO NPs acting as more potent apoptosis inducers than ZnO NRs. The strongest response to ZnO nanostructures was observed for caspase 2, a highly conserved apoptosis initiator caspase involved in the intrinsic (stress-induced) apoptosis [94]. Caspase 2 (found in the cytosol as well as the mitochondria [95]) is activated by p53 in response to genotoxic stimuli, metabolic imbalance or endoplasmic reticulum stress [94, 96]. Caspase 2 acts upstream of the classical, mitochondrially-induced intrinsic apoptosis pathways (triggered by mitochondrial membrane permeability transition (MMPT) and cytochrome c release) and may act as stimulator or inhibitor of apoptosis, depending on alternative splicing [96]. Earlier studies showed that stress-induced apoptosis in bivalves (such as caused by exposure to toxic metals Cu^{2+} or Cd^{2+}) does not involve MMPT or cytochrome c release [97, 98]. The mechanisms of this MMPT-independent apoptosis remain poorly understood in mollusks [97-99], and upregulation of caspase 2 might provide such putative apoptotic mechanism acting upstream of the MMPT-dependent pathway. The apoptosis activation by ZnO nanostructures was specific to the intrinsic stress-induced apoptosis pathway as there was no transcriptional activation of the main regulatory caspase of the extrinsic (death receptor-activated) caspase 8 [100]. Notably, mRNA expression of the main executor caspase, caspase 3, did not show a consistent response to nano-ZnO exposures. Transcript levels of caspase 3 were elevated in the mussels exposed to high concentrations of ZnO NPs, suppressed in those exposed to low concentrations of ZnO NPs, and did not change in the mussels exposed to ZnO NRs. Caspase 3 is an executor caspase acting downstream from the initiator caspases such

as caspase 2 and 8 [94, 100] and is typically activated by cleavage by initiator caspases [96]. Therefore, the predominantly posttranslational regulation of caspase 3 activity in apoptosis may explain the lack of consistent transcriptional response of this gene to apoptotic stimuli such as nano-ZnO [37, 96].

Caspase 2 was shown to be a potent activator of nuclear factor-κB (NF-κB) pathway in a marine bivalve *C. gigas* [101]. Our present study supports this notion and shows a coordinated pattern of upregulation of caspase 2 with NF-κB and TAK1 (Pearson correlation coefficient R=0.60 and R=0.59, respectively, $p<0.001$) in *Mytilus* exposed to ZnO nanostructures. TAK1 is a key intracellular kinase involved in the cross-talk between TGF-β and NF-κB pathways [102]. Furthermore, elevated expression of NF-κB and TAK1 was associated with upregulation of mRNA of Bcl-2, an antiapoptotic protein under the transcriptional control of NF-κB [103]. Exposure to ZnO NPs (but not NRs) stimulated mRNA expression of IKK2, a regulatory protein kinase which phosphorylates inhibitors of NF-κB (IκB) and targets them for degradation [103]. This releases NF-κB subunits and results in formation of transcriptionally active NF-κB dimers that translocate into the nucleus and activate target gens involved in cell survival, proliferation and inflammatory responses [103, 104]. Overall, our data indicate that exposure to ZnO nanostructure leads to a coordinated transcriptional upregulation of multiple targets of NF-κB pathway and suggests a pro-inflammatory effect of nano-ZnO exposures.

Unlike nano-ZnO, exposure to ionic Zn^{2+} at the same concentrations did not result in the activation of apoptotic cascades or the NF-κB pathways in *Mytilus*. Caspase 2 mRNA expression was downregulated in the mussels exposed to ionic Zn, whereas the levels of other apoptotic markers or inflammatory (NF-κB-related) did not change. This agrees with the established role of Zn^{2+} as an apoptotic inhibitor [105-108] and emphasizes the fundamental difference between the toxic mechanisms of Zn^{2+} and ZnO nanoparticles in the mussels.

Conclusions and outlook

Our study showed common toxic mechanisms of the studied forms of nano-ZnO, such as nanoparticles, attached and suspended nanorods that involve activation of apoptotic and inflammatory (NF-κB-related) pathways in a keystone marine bivalve and a common fouling organism, the blue mussel *M. edulis*. Pro-apoptotic action of nano-ZnO in the mussels reflects stimulation of intrinsic apoptotic pathways responding to the cellular injury and stress, rather than the death-ligand activated extrinsic pathways. These toxic mechanisms of nano-ZnO are fundamentally different from those of ionic Zn^{2+} exposures which showed no inflammatory response and suppression of the apoptotic pathways. Generally, the pro-apoptotic and pro-inflammatory action was stronger in the common commercial ZnO NPs compared with the novel ZnO nanorod structures developed as a potential antifouling

coating. High toxicity of attached ZnO nanorods (indicated by elevated mortality and stimulation of stress-induced caspase 2) may be explained by the 10-times higher concentration (12 μM) of ZnO in our experiment. Additionally, higher toxicity could be explained by the immediate impact of coatings on the mussels, since they were attached directly to coated substrates, while in other treatments nanostructures were dispersed in seawater. . Suspended ZnO nanorods were considerably less toxic, and the high concentrations of suspended ZnO NRs (1.2 μM) had similar biomarker profile to the low concentrations of ZnO NPs (0.12 μM). This finding agrees with the notion that the toxic effects of the nanomaterials critically depend on their size and shape [109]. Given the stability of ZnO NR coatings [9, 10] and the relatively low toxicity of ZnO NRs in suspensions, the undesirable effects of NR release due to the damage of the coating might be expected to be low in marine organisms such as mussels, making ZnO NR coating a potential low toxic alternative to copper-containing antifouling paints. Further investigations in marine organisms at different trophic levels (including primary producers and zooplankton) and at different concentrations of ZnO nanorods are needed to confirm the putative low off-target toxicity of ZnO NRs.

It is worth noting that traditional general stress biomarkers (such as oxidative lesions or lysosomal membrane destabilization) showed a relatively low power to detect the toxic effects of ZnO nanostructures or to distinguish between the stress effects caused by nanostructures and ionic Zn^{2+}. This indicates that molecular markers of apoptosis and inflammation (combined with the assessment of tissue Zn burdens) should be preferred choice for assessment of the stress from exposures to metal-containing nanomaterials. Our study also showed no metabolic imbalance caused by the exposures to nano-ZnO or Zn^{2+} indicating that the concentrations of Zn chosen for our experimental exposures (0.12 and 1.2 μM) do not cause extreme stress leading to bioenergetically non-sustainable state [39, 57]. Therefore, while ZnO-exposed mussels might suffer reduction in fitness, the tested concentrations of ZnO nanomaterials or ionic Zn^{2+} are likely compatible with the long-term population survival [39, 57].

ACKNOWLEDGEMENTS

This work was in part supported by Alexander von Humboldt Fellowship to HF and SD, and China Scholarship Council (CSC) to FW. SD acknowledged support of the TRC project [RC/AGR/FISH/16/01.

FIGURE CAPTIONS

Figure 1. Images of ZnO nanomaterials used in the present work.

- **I.** Scanning electron micrograph (SEM) images of (a) ZnO nanoparticles, (b) ZnO nanorods on glass substrate, and (c) free suspended ZnO nanorods collected from glass substrate.
- **II.** Transmission electron micrographs (TEM) of (a) ZnO nanoparticles, (b) high resolution imaging of a single ZnO nanoparticle, and (c) selected area diffraction (SAED) pattern of ZnO nanoparticles.
- **III.** TEM micrographs of (a) ZnO nanorods, (b) high resolution imaging on one rod, and (c) SAED pattern of a single ZnO nanorod.

Figure 2. Effects of nano-ZnO and Zn^{2+} exposures on levels of oxidative lesions, metallothioneins and cathepsin D in the whole body, and lysosomal membrane stability in hemocytes of *M. edulis*.

A – markers of lipid peroxidation (TBARS), B – protein oxidation markers (carbonyls), C – metallothioneins, D – index of the lysosomal membrane stability (neutral red retention time), E, F, - free and total cathepsin D activity, respectively. Different letters indicate values that are significantly different ($p<0.05$). If two columns share a letter, they are not significantly different ($p>0.05$). N=6.

Figure 3. Effects of nano-ZnO and Zn^{2+} exposures on the body levels of energy reserves in *M. edulis*.

A – lipids, B – carbohydrates, C – proteins, D – total energy content of the body. Different letters indicate values that are significantly different ($p<0.05$). If two columns share a letter, they are not significantly different ($p>0.05$). N=6.

Figure 4. Effects of nano-ZnO and Zn^{2+} exposures on the activity of mitochondrial ETS and non-mitochondrial reductases in the body of *M. edulis*.

A – ETS activity, B – non-mitochondrial reductase activity. Different letters indicate values that are significantly different ($p<0.05$). If two columns share a letter, they are not significantly different ($p>0.05$). N=6.

Figure 5. Effects of nano-ZnO and Zn^{2+} exposures on expression of the target genes in apoptosis and cell survival pathways in the body of *M. edulis*.

Different letters indicate values that are significantly different ($p<0.05$). If two columns share a letter, they are not significantly different ($p>0.05$). N=6.

Figure 6. Principal component analysis of the biochemical and molecular biomarkers of stress and energy metabolism in *M. edulis*.

Biomarker abbreviations: Cas2 – caspase 2; Cas3 – caspase 3; Cas8 – caspase 8; Bcl-2 - B-cell lymphoma 2; BAX - Bcl-2-associated X protein; TAK1 - TGF-β-activated kinase 1; NF- κB – nuclear factor κB a; IKK1 - inhibitor of NF-κB kinase-1; IKK2 - inhibitor of NF-κB kinase-2; ETS – electron transport system activity; Non-mito – activity of non-mitochondrial reductases; Prot – body protein content; CarbH - body carbohydrates content; Lip - body lipid content; ER – total energy reserves; CEA – cellular energy allocation; MTs – metallothioneins; NRR – neutral red retention time; PC – protein carbonyls; TBARS- thiobarbituric acid-reactive substances; CathDt and CathDf – total and free cathepsin D activity, respectively.

Experimental treatment groups: C – control, NP-L and NP-H – low and high concentrations of ZnO NPs (0.12 and 1.2 μM Zn, respectively); NR-L and NR-H - low and high concentrations of ZnO NRs (0.12 and 1.2 μM Zn, respectively); NRa – attached nanorods: Zn-L and Zn-H - low and high concentrations of Zn^{2+} (0.12 and 1.2 μM, respectively).

Figure 7. Integrated biomarker radar plot for bioenergetics-related biomarkers in *M. edulis*.

Biomarker abbreviations: ETS – electron transport system activity; Nn.m – activity of non-mitochondrial reductases; Prot – body protein content; CarbH - body carbohydrates content; Lip - body lipid content; ER – total energy reserves; CEA – cellular energy allocation.

Experimental treatment groups: C – control, NPL and NPH – low and high concentrations of ZnO NPs (0.12 and 1.2 μM Zn, respectively); NRL and NRH - low and high concentrations of ZnO NRs (0.12 and 1.2 μM Zn, respectively); NRA – attached nanorods: ZnL and ZnH - low and high concentrations of Zn^{2+} (0.12 and 1.2 μM, respectively).

Figure 8. Integrated biomarker radar plot for oxidative stress and general stress biomarkers in *M. edulis*.

Biomarker abbreviations: MTs – metallothioneins; NRR – neutral red retention time; PC – protein carbonyls; TBARS- thiobarbituric acid-reactive substances; CtD and CD – total and free cathepsin D activity, respectively.

Experimental treatment groups: C – control, NPL and NPH – low and high concentrations of ZnO NPs (0.12 and 1.2 μM Zn, respectively); NRL and NRH - low and high concentrations of

ZnO NRs (0.12 and 1.2 μM Zn, respectively); NRA – attached nanorods: ZnL and ZnH - low and high concentrations of Zn^{2+} (0.12 and 1.2 μM, respectively).

Figure 9. Integrated biomarker radar plot for molecular apoptosis- and inflammation-related biomarkers in *M. edulis*.

Biomarker abbreviations: Bcl2 - B-cell lymphoma 2; BAX - Bcl-2-associated X protein; TGFk - TGF-β-activated kinase 1; NFKb – nuclear factor κB a; Cas2 – caspase 2; Cas3 – caspase 3; Cas8 – caspase 8.

Experimental treatment groups: C – control, NPL and NPH – low and high concentrations of ZnO NPs (0.12 and 1.2 μM Zn, respectively); NRL and NRH - low and high concentrations of ZnO NRs (0.12 and 1.2 μM Zn, respectively); NRA – attached nanorods: ZnL and ZnH - low and high concentrations of Zn^{2+} (0.12 and 1.2 μM, respectively).

Figure 10. CART analysis of biomarkers separating different experimental treatment groups of *M. edulis*.

Biomarker abbreviations: Cas2 – caspase 2; Cas8 – caspase 8; Lip – body lipid content; IKK2 - inhibitor of NF-κB kinase-2.

Experimental treatment groups: C – control, NPL and NPH – low and high concentrations of ZnO NPs (0.12 and 1.2 μM Zn, respectively); NRL and NRH - low and high concentrations of ZnO NRs (0.12 and 1.2 μM Zn, respectively); NRA – attached nanorods: ZnL and ZnH - low and high concentrations of Zn^{2+} (0.12 and 1.2 μM, respectively).

I

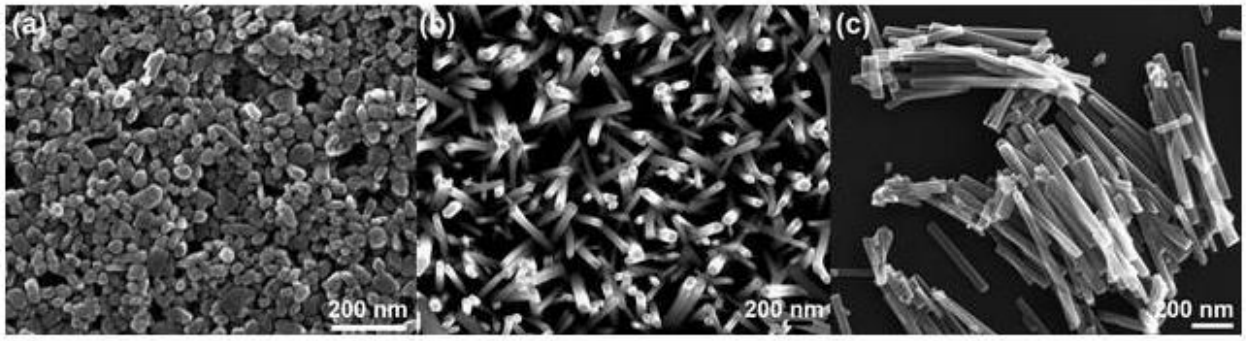

II

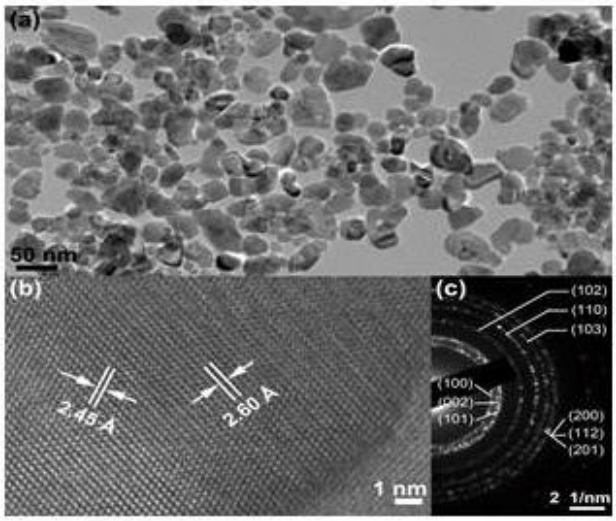

III

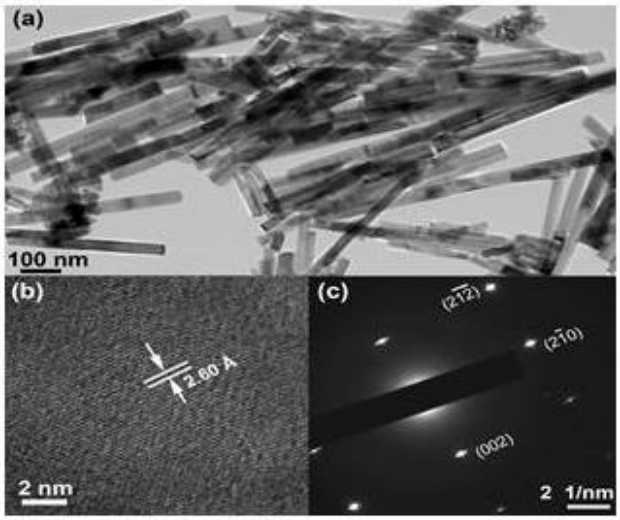

Figure 1

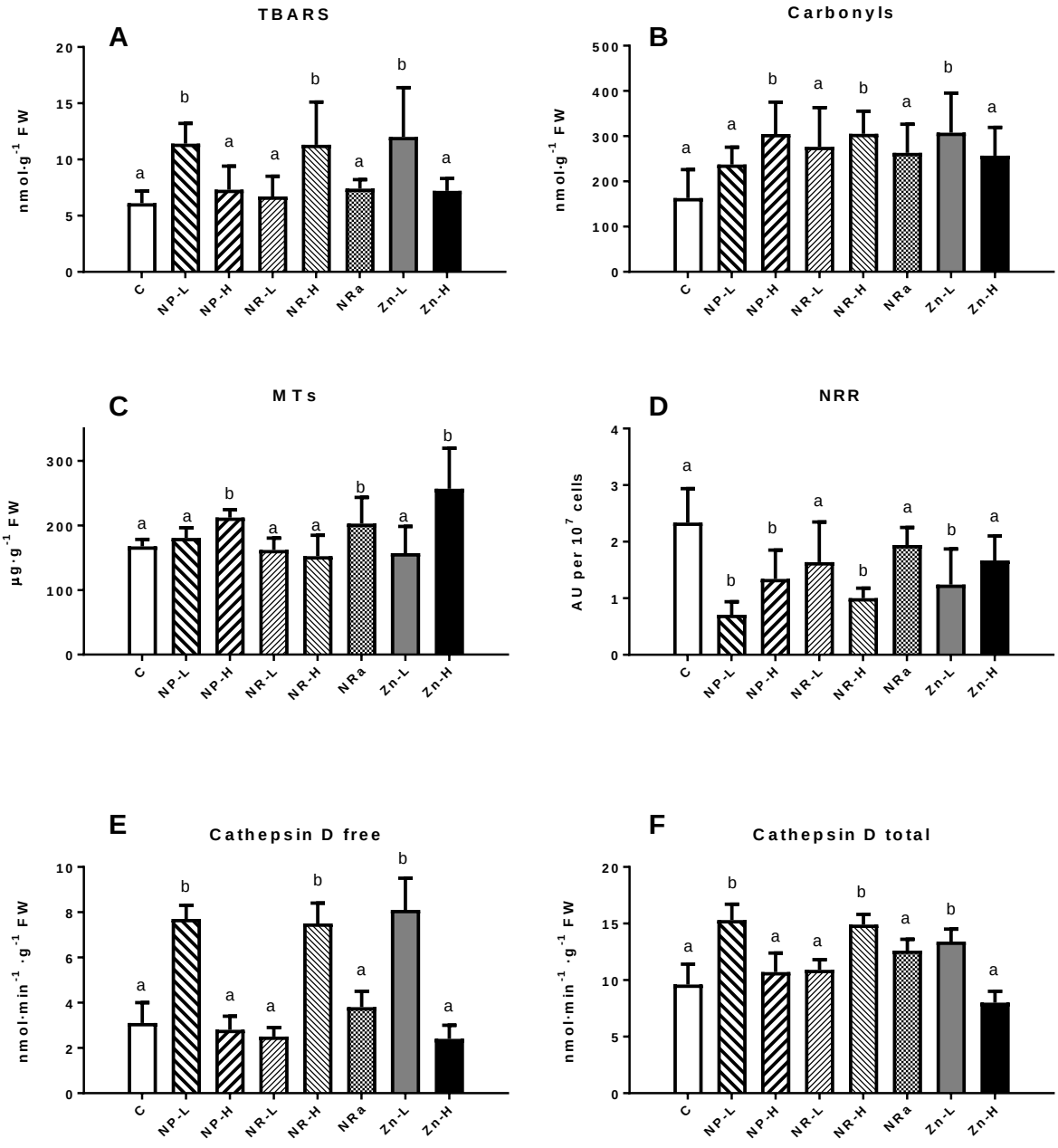
A
TBARS
nmol·g-1 FW
B
Carbonyls
nmol·g-1 FW
C
MTs
µg·g-1 FW
D
NRR
AU per 10^7 cells
E
Cathepsin D free
nmol·min-1·g-1 FW
F
Cathepsin D total
nmol·min-1·g-1 FW
C
NP-L
NP-H
NR-L
NR-H
NRa
Zn-L
Zn-H

Figure 2

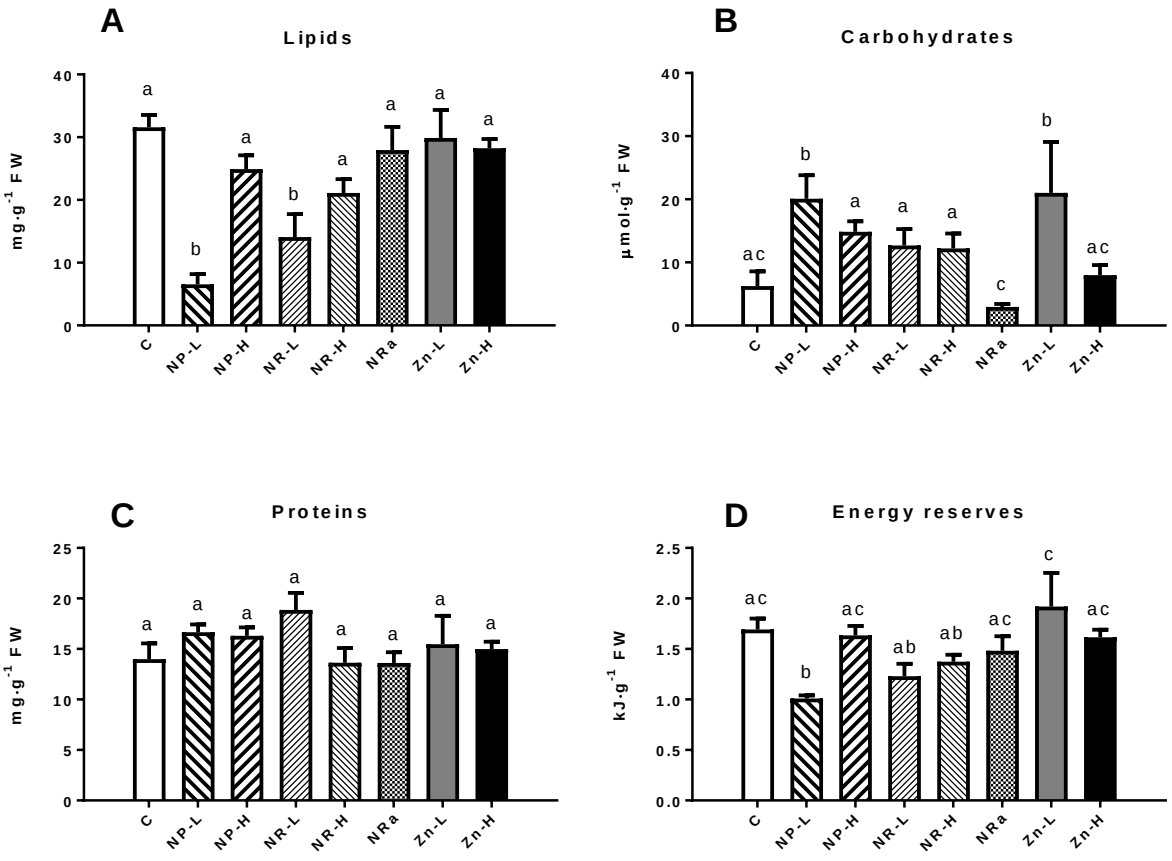
A
Lipids
mg·g-1 FW
40
30
20
10
0
a
b
a
b
a
a
a
a
C
NP-L
NP-H
NR-L
NR-H
NRa
Zn-L
Zn-H
B
Carbohydrates
µmol·g-1 FW
40
30
20
10
0
ac
b
a
a
a
c
b
ac
C
NP-L
NP-H
NR-L
NR-H
NRa
Zn-L
Zn-H
C
Proteins
mg·g-1 FW
25
20
15
10
5
0
a
a
a
a
a
a
a
a
C
NP-L
NP-H
NR-L
NR-H
NRa
Zn-L
Zn-H
D
Energy reserves
kJ·g-1 FW
2.5
2.0
1.5
1.0
0.5
0.0
ac
b
ac
ab
ab
ac
c
ac
C
NP-L
NP-H
NR-L
NR-H
NRa
Zn-L
Zn-H

Figure 3

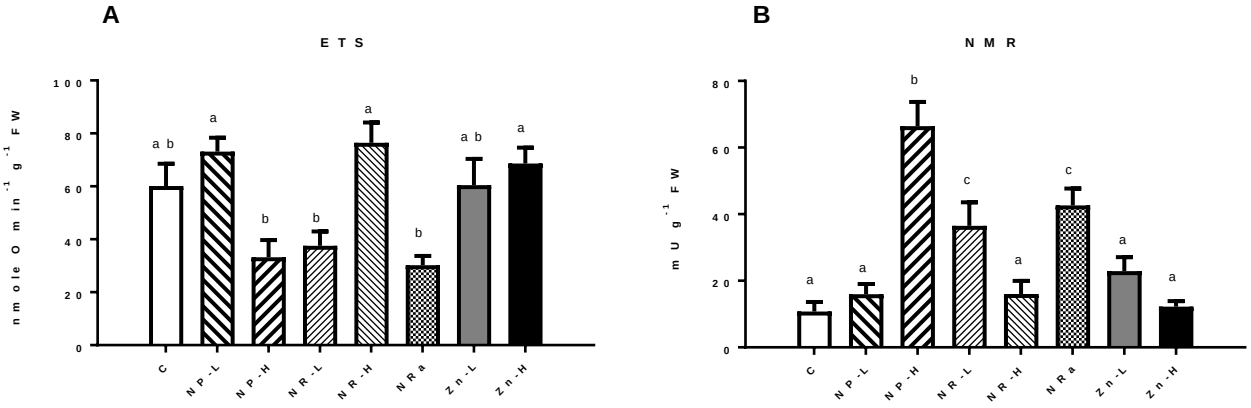
A
ETS
nmole O min-1 g-1 FW
100
80
60
40
20
0
a b
a
b
b
a
b
a b
a
C
NP -L
NP -H
NR -L
NR -H
NRa
Zn -L
Zn -H
B
NMR
mU g-1 FW
80
60
40
20
0
a
a
b
c
a
c
a
a
C
NP -L
NP -H
NR -L
NR -H
NRa
Zn -L
Zn -H

Figure 4

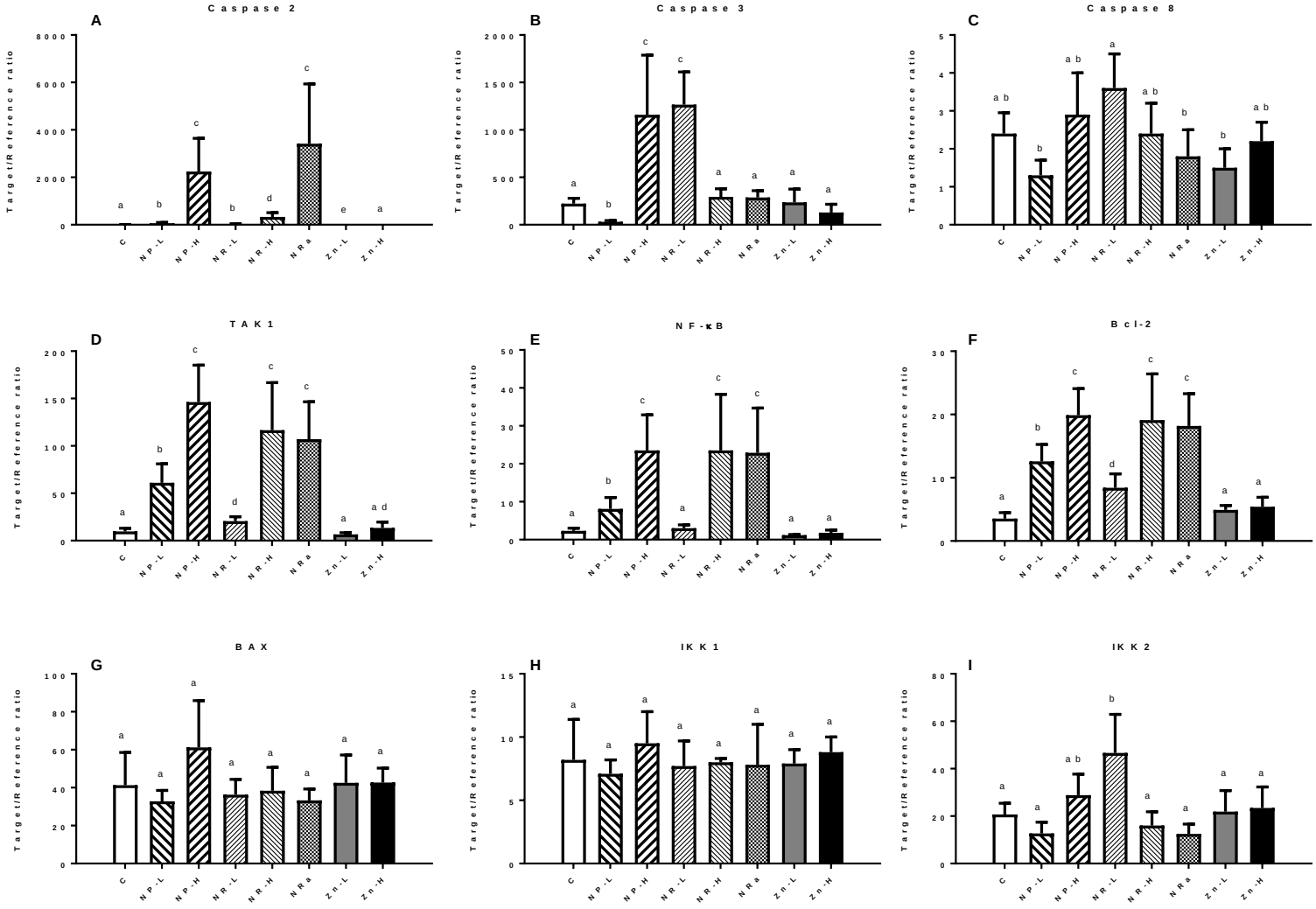
A
Caspase 2
B
Caspase 3
C
Caspase 8
D
TAK1
E
NF-κB
F
Bcl-2
G
BAX
H
IKK1
I
IKK2
Target/Reference ratio
C
NP-L
NP-H
NR-L
NR-H
NRa
Zn-L
Zn-H

Figure 5

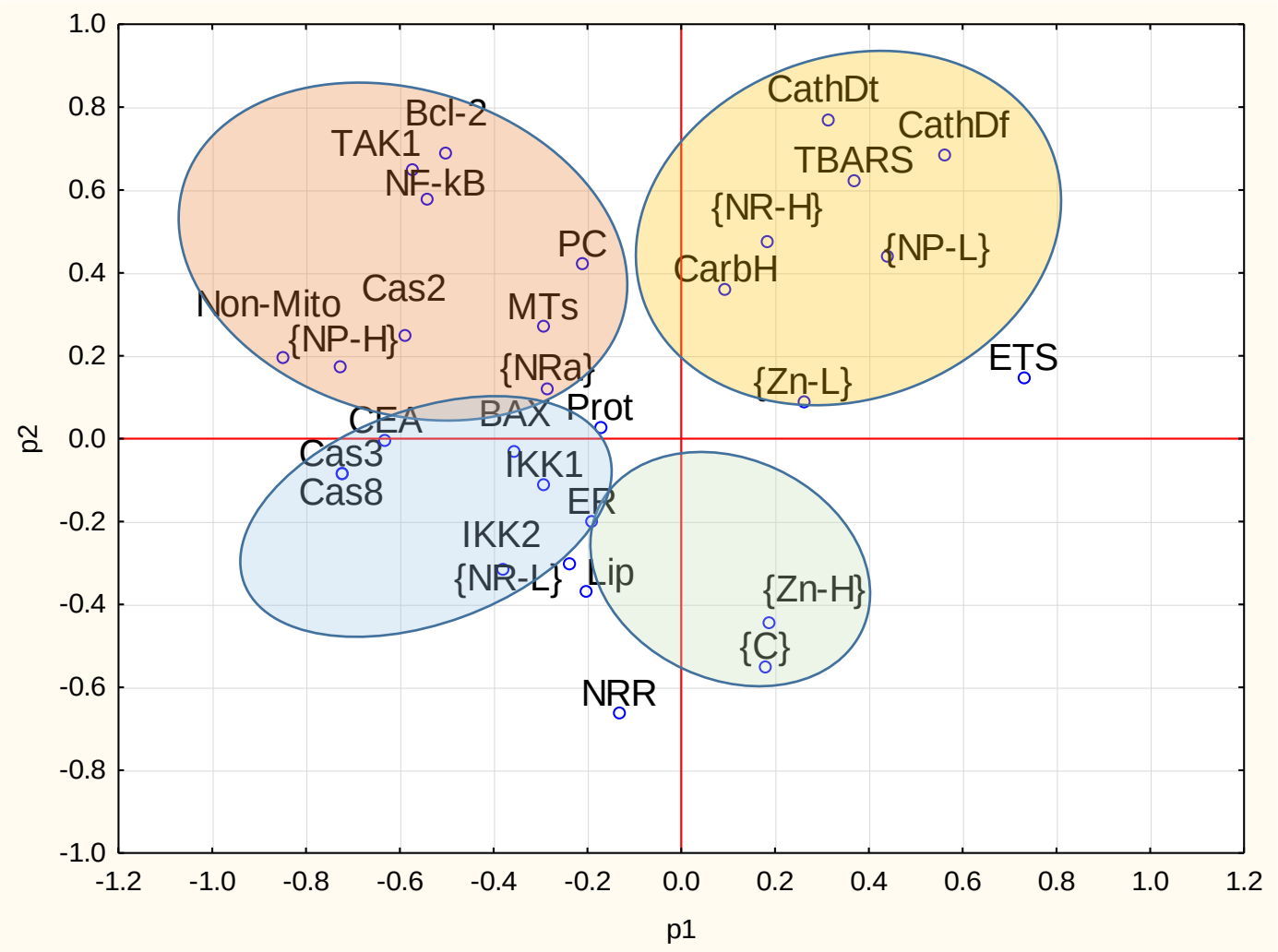
1.0
0.8
0.6
0.4
0.2
0.0
-0.2
-0.4
-0.6
-0.8
-1.0
p2
-1.2
-1.0
-0.8
-0.6
-0.4
-0.2
0.0
0.2
0.4
0.6
0.8
1.0
1.2
p1
Bcl-2
TAK1
NF-kB
PC
Cas2
Non-Mito
MTs
{NP-H}
{NRa}
CEA
BAX
Prot
Cas3
Cas8
IKK1
ER
IKK2
{NR-L}
Lip
NRR
CathDt
CathDf
TBARS
{NR-H}
{NP-L}
CarbH
ETS
{Zn-L}
{Zn-H}
{C}

Figure 6

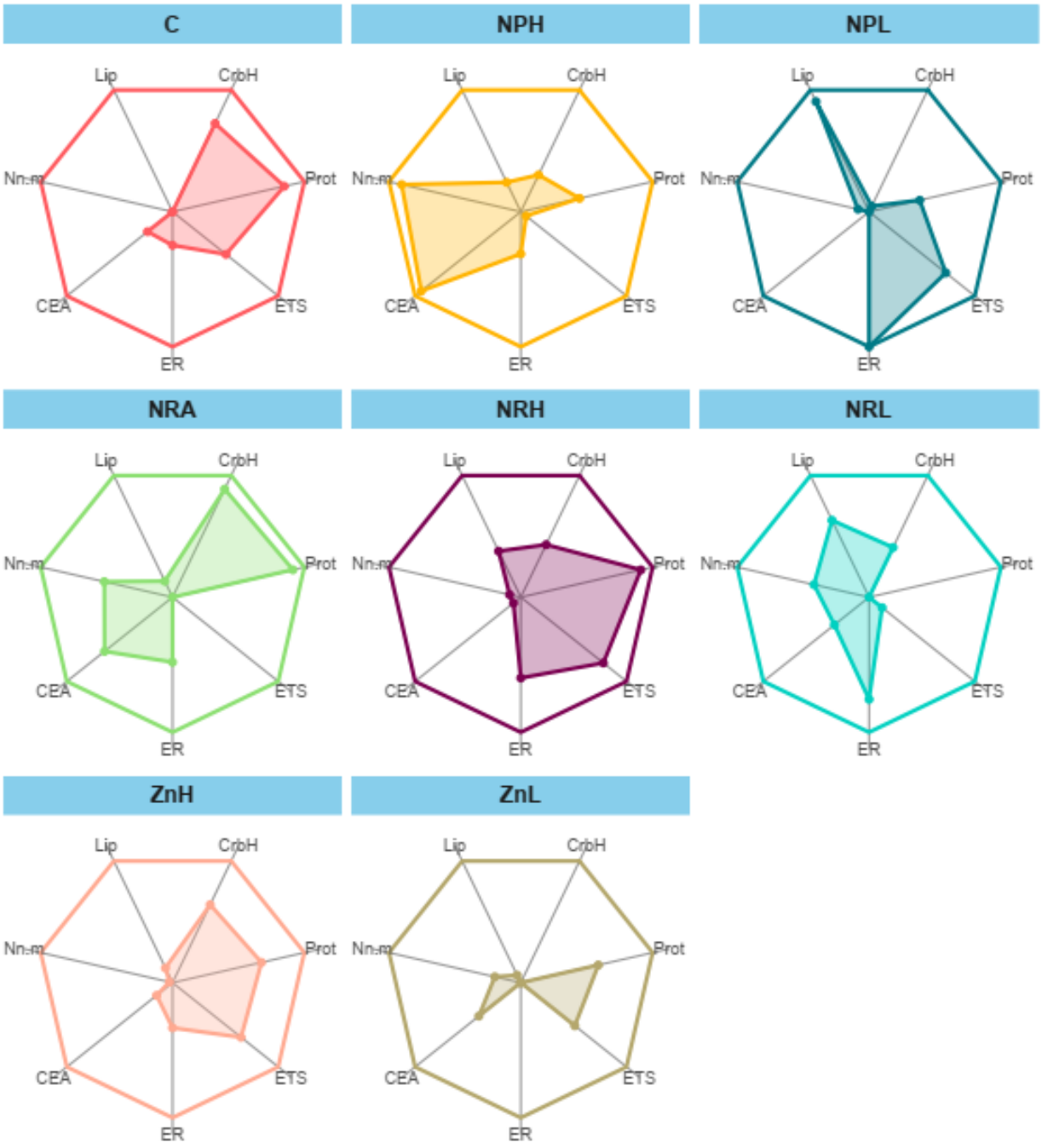

Figure 7

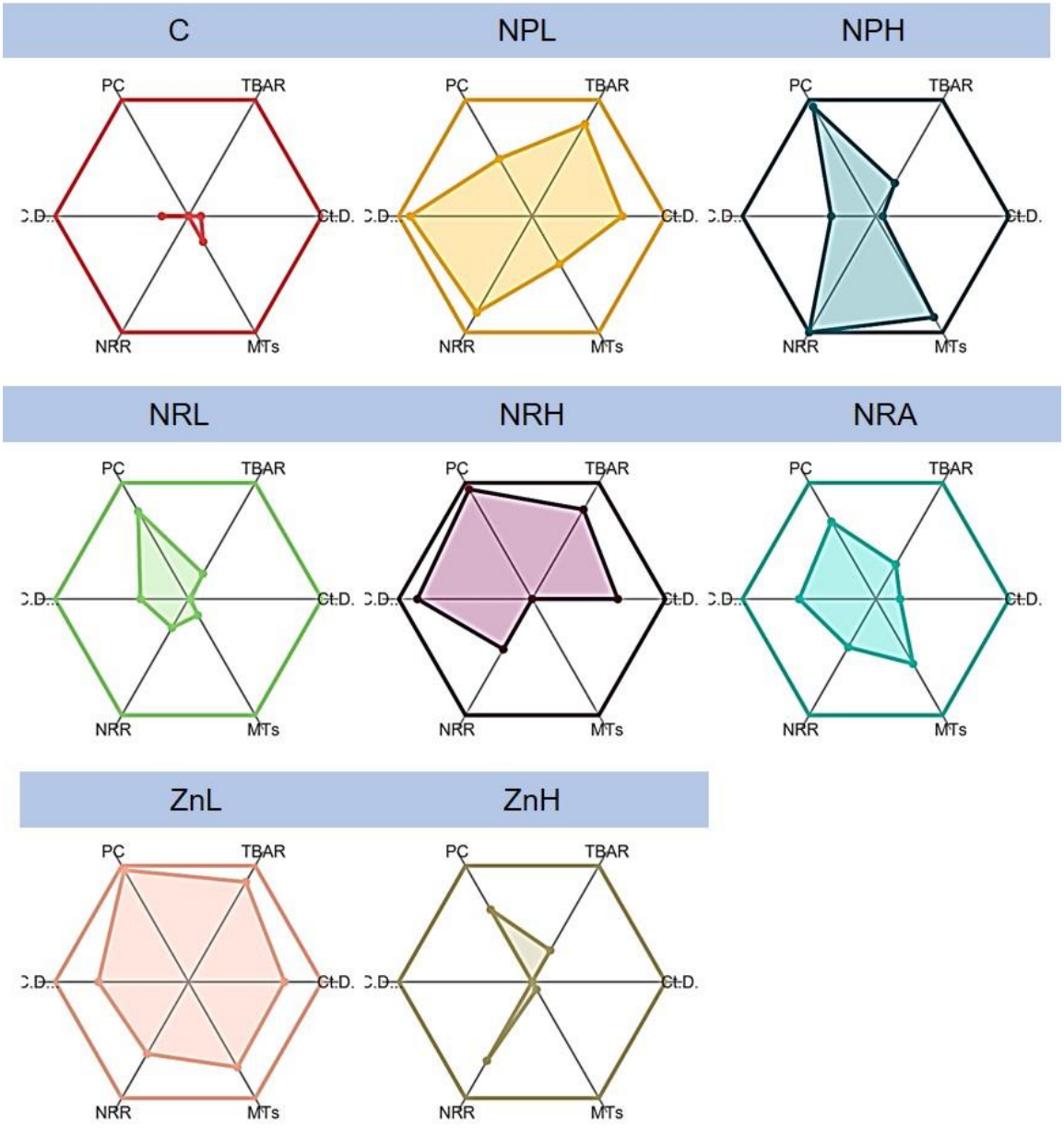

Figure 8

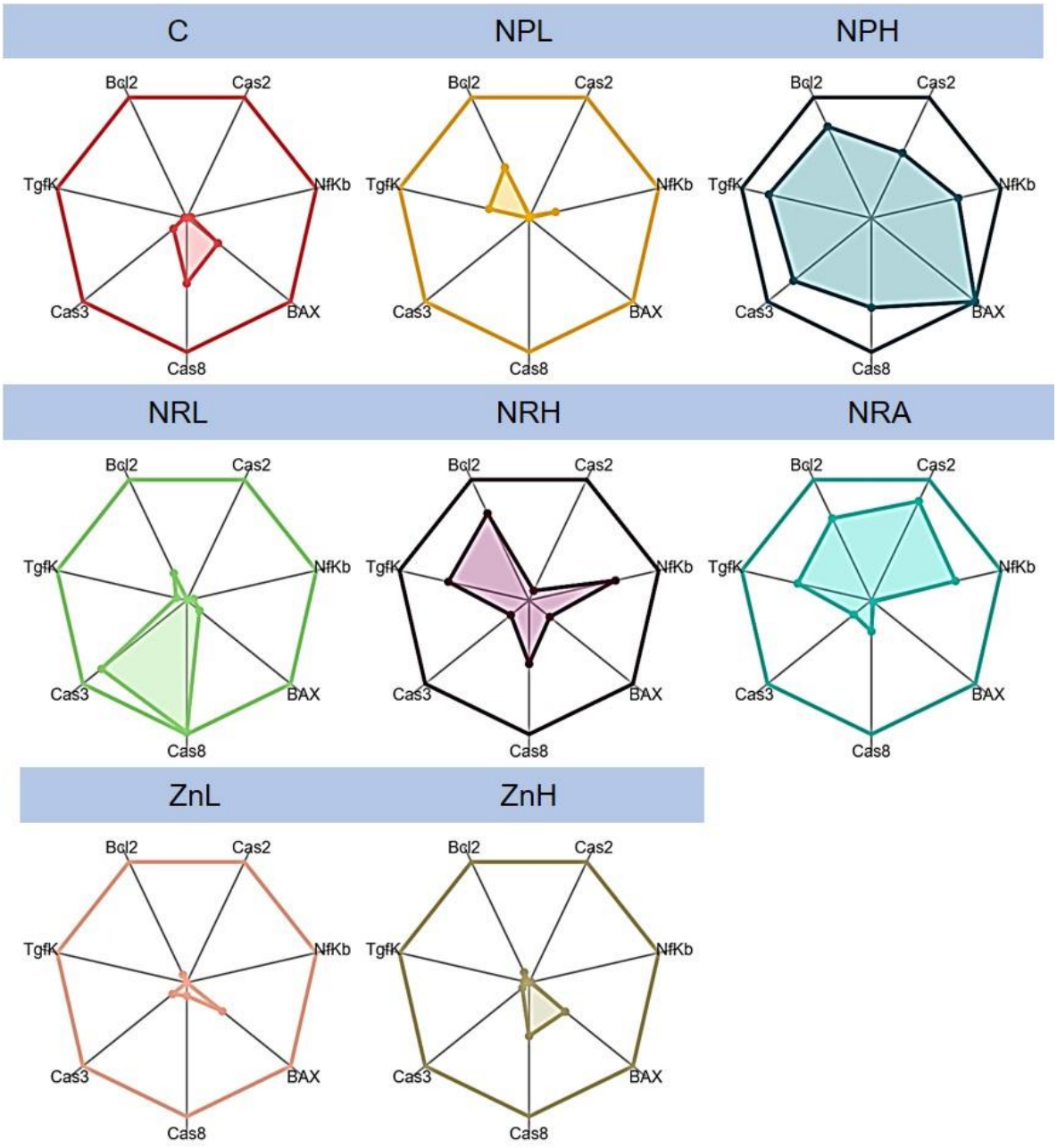

Figure 9

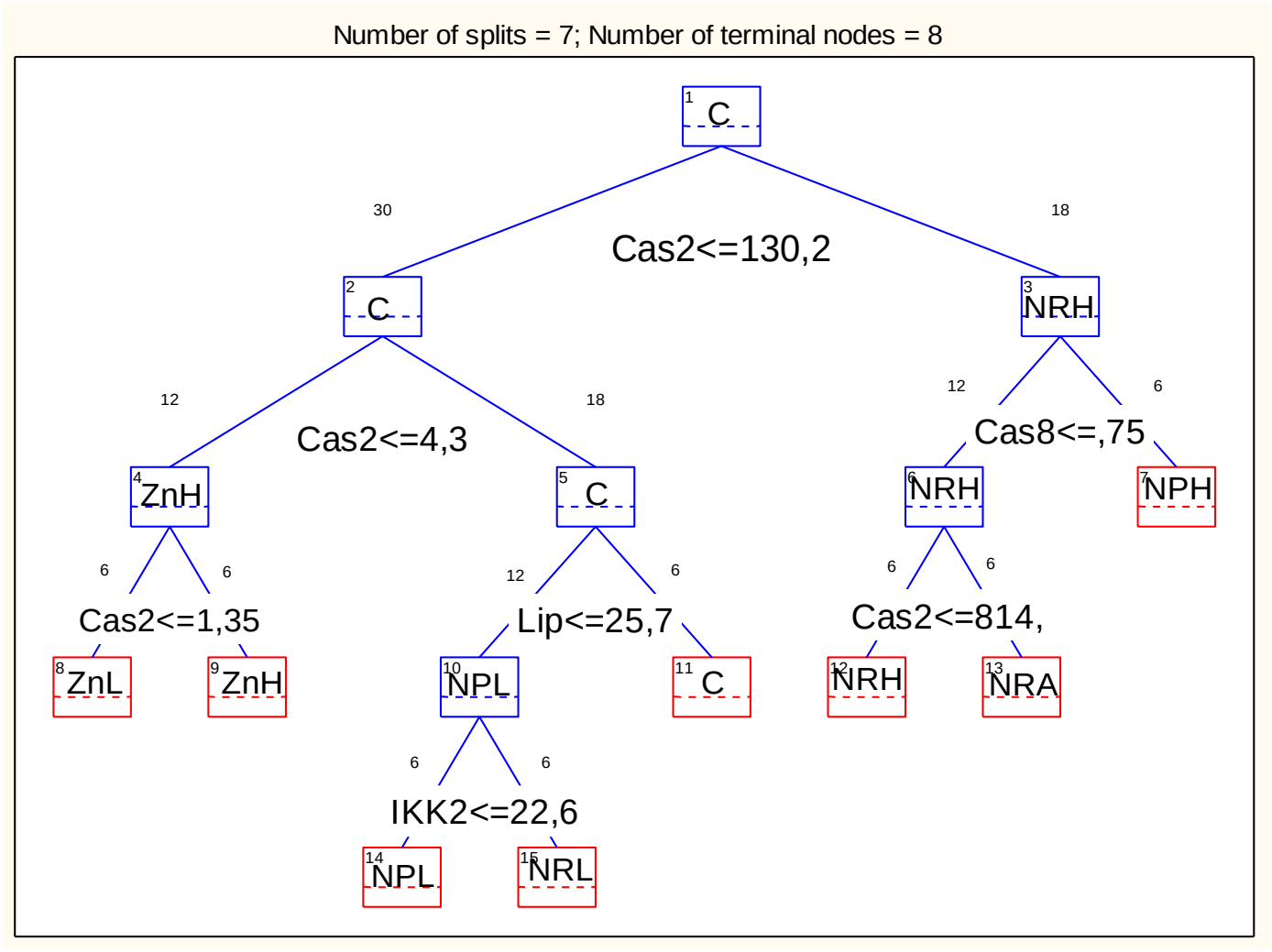
Number of splits = 7; Number of terminal nodes = 8
1 C
30
Cas2<=130,2
18
2 C
3 NRH
12
Cas2<=4,3
18
12
Cas8<=,75
6
4 ZnH
5 C
6 NRH
7 NPH
6
6
12
6
6
6
Cas2<=1,35
Lip<=25,7
Cas2<=814,
8 ZnL
9 ZnH
10 NPL
11 C
12 NRH
13 NRA
6
6
IKK2<=22,6
14 NPL
15 NRL

Figure 10

Table 1. Primer sequences for the target and housekeeping genes

Gene abbreviations: Bcl-2 - B-cell lymphoma 2; BAX - Bcl-2-associated X protein; TAK1 - TGF-β-activated kinase 1; NF-κB – nuclear factor κBa (p100/p105); IKK1 - inhibitor of NF-κB kinase-1; IKK2 - inhibitor of NF-κB kinase-2; EF1 – eukaryotic elongation factor 1α.

Gene	Forward primer (3'-5')	Reverse primer (3'-5')	NCBI accession #
Caspase 2	ACAAGTGCAGATGCTGTGTTG	ACACCTCTCACATTGTCGGC	HQ424449.1
Caspase 3	ACGACAGCTAGTTCACCAGG	CCACCAGAAGAGGAGTTCCG	HQ424453.1
Caspase 8	AATGTCGGTACCCCACGATG	CGTGTATGAACCATGCCCCT	HQ424450.1
Bcl-2	CGGTGGTTGGCAAGGATTTG	CGCCATTGCGCCTATTACAC	KC545829.1
BAX	TAACTGGGGACGTGTAGGCA	CCAGGGGGCGACATAATCTG	KC545830.1
TAK1	CACCAAACCGAACTGGACCT	GGAACTGCTGTGATCCGACA	KF015298.1
NF-κB	TGGATGATGAGGCCAAACCC	TGAAGTCCACCATGTGACGG	KF051275.1
IKK1	GTGGCCACCAGTCAAGTGAT	TAAGGCTGCAGCTTGCTGAT	KF015301.1
IKK2	TGCAGGAGCCGATAAAGCAA	CCGCCGGAACAAAATTCCAT	KF015302.1
EF1	GACAGCAAAAACGACCCACC	TTCTCCAGGGTGGTTCAGGA	AF063420

REFERENCES

[1] R.J. Williams, S. Harrison, V. Keller, J. Kuenen, S. Lofts, A. Praetorius, C. Svendsen, L.C. Vermeulen, J. van Wijnen, Models for assessing engineered nanomaterial fate and behaviour in the aquatic environment, Current Opinion in Environmental Sustainability, 36 (2019) 105-115.
[2] P. Sathe, K. Laxman, M.T.Z. Myint, S. Dobretsov, J. Richter, J. Dutta, Bioinspired nanocoatings for biofouling prevention by photocatalytic redox reactions, Scientific reports, 7 (2017) 3624-3624.
[3] M. Wahl, Marine epibiosis. I. Fouling and antifouling: some basic aspects, Marine Ecology Progress Series, 58 (1989) 175-189.
[4] Y. Sapozhnikova, E. Wirth, K. Schiff, M. Fulton, Antifouling biocides in water and sediments from California marinas, Mar Pollut Bull, 69 (2013) 189-194.
[5] N. Tsunemasa, H. Yamazaki, Concentration of antifouling biocides and metals in sediment core samples in the northern part of Hiroshima Bay, International journal of molecular sciences, 15 (2014) 9991-10004.
[6] S.J. Brooks, M. Waldock, Copper Biocides in the Marine Environment, in: T. Arai, H. Harino, M. Ohji, W.J. Langston (Eds.) Ecotoxicology of Antifouling Biocides, Springer Japan, Tokyo, 2009, pp. 413-428.
[7] M. Inoue, A. Suzuki, M. Nohara, H. Kan, A. Edward, H. Kawahata, Coral skeletal tin and copper concentrations at Pohnpei, Micronesia: possible index for marine pollution by toxic anti-biofouling paints, Environmental Pollution, 129 (2004) 399-407.
[8] P. Sathe, J. Richter, M.T. Myint, S. Dobretsov, J. Dutta, Self-decontaminating photocatalytic zinc oxide nanorod coatings for prevention of marine microfouling: a mesocosm study, Biofouling, 32 (2016) 383-395.
[9] M. Al-Fori, S. Dobretsov, M.T. Myint, J. Dutta, Antifouling properties of zinc oxide nanorod coatings, Biofouling, 30 (2014) 871-882.
[10] S. Baruah, J. Dutta, Hydrothermal growth of ZnO nanostructures, Science and technology of advanced materials, 10 (2009) 013001.
[11] S.S. Mathiesen, J. Thyrring, J. Hemmer-Hansen, J. Berge, A. Sukhotin, P. Leopold, M. Bekaert, M.K. Sejr, E.E. Nielsen, Genetic diversity and connectivity within Mytilus spp. in the subarctic and Arctic, Evolutionary Applications, 10 (2017) 39-55.
[12] T. Kijewski, B. Śmietanka, M. Zbawicka, E. Gosling, H. Hummel, R. Wenne, Distribution of Mytilus taxa in European coastal areas as inferred from molecular markers, Journal of Sea Research, 65 (2011) 224-234.
[13] J. Beyer, N.W. Green, S. Brooks, I.J. Allan, A. Ruus, T. Gomes, I.L.N. Bråte, M. Schøyen, Blue mussels (*Mytilus edulis* spp.) as sentinel organisms in coastal pollution monitoring: A review, Marine Environmental Research, 130 (2017) 338-365.
[14] S. Bricker, G. Lauenstein, K. Maruya, NOAA's Mussel Watch Program: Incorporating contaminants of emerging concern (CECs) into a long-term monitoring program, Marine Pollution Bulletin, 81 (2014) 289-290.
[15] H. Falfushynska, E.P. Sokolov, F. Haider, C. Oppermann, U. Kragl, W. Ruth, M. Stock, S. Glufke, E.J. Winkel, I.M. Sokolova, Effects of a common pharmaceutical, atorvastatin, on energy metabolism and detoxification mechanisms of a marine bivalve Mytilus edulis, Aquatic Toxicology, 208 (2019) 47-61.
[16] C. González-Fernández, M. Albentosa, I. Sokolova, Interactive effects of nutrition, reproductive state and pollution on molecular stress responses of mussels, Mytilus galloprovincialis Lamarck, 1819, Marine Environmental Research, 131 (2017) 103-115.
[17] E. Blanco-Rayón, L. Guilhermino, M. Irazola, A.V. Ivanina, I.M. Sokolova, U. Izagirre, I. Marigómez, The influence of short-term experimental fasting on biomarker responsiveness in oil WAF exposed mussels, Aquatic Toxicology, 206 (2019) 164-175.
[18] I. Marigómez, M. Múgica, U. Izagirre, I.M. Sokolova, Chronic environmental stress enhances tolerance to seasonal gradual warming in marine mussels, PLOS ONE, 12 (2017) e0174359.

[19] M. Múgica, I.M. Sokolova, U. Izagirre, I. Marigómez, Season-dependent effects of elevated temperature on stress biomarkers, energy metabolism and gamete development in mussels, Marine Environmental Research, 103 (2015) 1-10.
[20] C.R. Newell, S.E. Shumway, Grazing of Natural Particulates by Bivalve Molluscs: A Spatial and Temporal Perspective, in, Springer Berlin Heidelberg, Berlin, Heidelberg, 1993, pp. 85-148.
[21] T. Strohmeier, Ø. Strand, M. Alunno-Bruscia, A. Duinker, P.J. Cranford, Variability in particle retention efficiency by the mussel *Mytilus edulis*, Journal of Experimental Marine Biology and Ecology, 412 (2012) 96-102.
[22] H.I. Falfushynska, L.L. Gnatyshyna, A.V. Ivanina, V.V. Khoma, O.B. Stoliar, I.M. Sokolova, Bioenergetic responses of freshwater mussels Unio tumidus to the combined effects of nano-ZnO and temperature regime, Science of The Total Environment, 650 (2019) 1440-1450.
[23] H. Falfushynska, L. Gnatyshyna, I. Yurchak, I. Sokolova, O. Stoliar, The effects of zinc nanooxide on cellular stress responses of the freshwater mussels Unio tumidus are modulated by elevated temperature and organic pollutants, Aquatic Toxicology, 162 (2015) 82-93.
[24] J. Hou, Y. Wu, X. Li, B. Wei, S. Li, X. Wang, Toxic effects of different types of zinc oxide nanoparticles on algae, plants, invertebrates, vertebrates and microorganisms, Chemosphere, 193 (2018) 852-860.
[25] H. Ma, P.L. Williams, S.A. Diamond, Ecotoxicity of manufactured ZnO nanoparticles--a review, Environmental pollution (Barking, Essex : 1987), 172 (2013) 76-85.
[26] T. Xia, M. Kovochich, M. Liong, L. Mädler, B. Gilbert, H. Shi, J.I. Yeh, J.I. Zink, A.E. Nel, Comparison of the mechanism of toxicity of zinc oxide and cerium oxide nanoparticles based on dissolution and oxidative stress properties, ACS nano, 2 (2008) 2121-2134.
[27] Y. Xiao, M.G. Vijver, G. Chen, W.J.G.M. Peijnenburg, Toxicity and Accumulation of Cu and ZnO Nanoparticles in Daphnia magna, Environmental Science & Technology, 49 (2015) 4657-4664.
[28] H. Falfushynska, L. Gnatyshyna, O. Horyn, I. Sokolova, O. Stoliar, Endocrine and cellular stress effects of zinc oxide nanoparticles and nifedipine in marsh frogs Pelophylax ridibundus, Aquatic Toxicology, 185 (2017) 171-182.
[29] Y. Shang, X. Wang, H. Kong, W. Huang, M. Hu, Y. Wang, Nano-ZnO Impairs Anti-predation Capacity of Marine Mussels under Seawater Acidification, Journal of Hazardous Materials, (2019).
[30] J. Li, S. Schiavo, D. Xiangli, G. Rametta, M.L. Miglietta, M. Oliviero, W. Changwen, S. Manzo, Early ecotoxic effects of ZnO nanoparticle chronic exposure in Mytilus galloprovincialis revealed by transcription of apoptosis and antioxidant-related genes, Ecotoxicology, 27 (2018) 369-384.
[31] S. Schiavo, M. Oliviero, J. Li, S. Manzo, Testing ZnO nanoparticle ecotoxicity: linking time variable exposure to effects on different marine model organisms, Environmental science and pollution research international, 25 (2018) 4871-4880.
[32] D. Shalini, S. Senthilkumar, P. Rajaguru, Effect of size and shape on toxicity of zinc oxide (ZnO) nanomaterials in human peripheral blood lymphocytes, Toxicol Mech Methods, 28 (2018) 87-94.
[33] T.O. Okyay, R.K. Bala, H.N. Nguyen, R. Atalay, Y. Bayam, D.F. Rodrigues, Antibacterial properties and mechanisms of toxicity of sonochemically grown ZnO nanorods, RSC Advances, 5 (2015) 2568-2575.
[34] I. Rago, C.R. Chandraiahgari, M.P. Bracciale, G. De Bellis, E. Zanni, M. Cestelli Guidi, D. Sali, A. Broggi, C. Palleschi, M. Sarto, D. Uccelletti, ZnO Microrods and Nanorods; Different Antibacterial activity and their mode of Action against Gram positive bacteria, in, 2014.
[35] X. Peng, S. Palma, N.S. Fisher, S.S. Wong, Effect of morphology of ZnO nanostructures on their toxicity to marine algae, Aquatic Toxicology, 102 (2011) 186-196.
[36] R.A. Goncalves, A.L. de Oliveira Franco Rossetto, D.J. Nogueira, D.S. Vicentini, W.G. Matias, Comparative assessment of toxicity of ZnO and amine-functionalized ZnO nanorods toward Daphnia magna in acute and chronic multigenerational tests, Aquat Toxicol, 197 (2018) 32-40.
[37] R.J. Vandebriel, W.H. De Jong, A review of mammalian toxicity of ZnO nanoparticles, Nanotechnology, science and applications, 5 (2012) 61-71.

[38] A. Nel, T. Xia, L. Madler, N. Li, Toxic Potential of Materials at the Nanolevel, Science, 311 (2006) 622-627.
[39] I.M. Sokolova, Energy-Limited Tolerance to Stress as a Conceptual Framework to Integrate the Effects of Multiple Stressors, Integrative and Comparative Biology 53 (2013) 597-608.
[40] D. Glick, S. Barth, K.F. Macleod, Autophagy: cellular and molecular mechanisms, J Pathol, 221 (2010) 3-12.
[41] D.G. Perez, C.S. Fontanetti, Hemocitical responses to environmental stress in invertebrates: a review, Environmental Monitoring and Assessment, 177 (2010) 437-447.
[42] J.C. Amiard, C. Amiard-Triquet, S. Barka, J. Pellerin, P.S. Rainbow, Metallothioneins in aquatic invertebrates: Their role in metal detoxification and their use as biomarkers, Aquatic Toxicology, 76 (2006) 160-202.
[43] H. Stuckas, L. Knöbel, H. Schade, C. Breusing, H.-H. Hinrichsen, M. Bartel, K. Langguth, F. Melzner, Combining hydrodynamic modelling with genetics: can passive larval drift shape the genetic structure of Baltic Mytilus populations?, Molecular Ecology, 26 (2017) 2765-2782.
[44] H. Ohkawa, N. Ohishi, K. Yagi, Assay for lipid peroxides in animal tissues by thiobarbituric acid reaction, Analytical Biochemistry, 95 (1979) 351-358.
[45] A.Z. Reznick, L. Packer, Oxidative damage to proteins: spectrophotometric method for carbonyl assay, Methods Enzymol, 233 (1994) 357-363.
[46] A. Viarengo, E. Ponzano, F. Dondero, R. Fabbri, A simple spectrophotometric method for metallothionein evaluation in marine organisms: an application to Mediterranean and Antarctic molluscs, Marine Environmental Research, 44 (1997) 69-84.
[47] J.T. Dingle, A.J. Barrett, P.D. Weston, Cathepsin D. Characteristics of immunoinhibition and the confirmation of a role in cartilage breakdown, Biochem J, 123 (1971) 1-13.
[48] E. Van Handel, Rapid determination of total lipids in mosquitoes, Journal of the American Mosquito Control Association, 1 (1985) 302-304.
[49] T. Masuko, A. Minami, N. Iwasaki, T. Majima, S.-I. Nishimura, Y.C. Lee, Carbohydrate analysis by a phenol–sulfuric acid method in microplate format, Analytical Biochemistry, 339 (2005) 69-72.
[50] E. Gnaiger, Calculation of Energetic and Biochemical Equivalents of Respiratory Oxygen Consumption, in: E. Gnaiger, H. Forstner (Eds.) Polarographic Oxygen Sensors: Aquatic and Physiological Applications, Springer Berlin Heidelberg, Berlin, Heidelberg, 1983, pp. 337-345.
[51] W.M. De Coen, C.R. Janssen, The use of biomarkers in Daphnia magna toxicity testing. IV. Cellular Energy Allocation: a new methodology to assess the energy budget of toxicant-stressed *Daphnia* populations, Journal of Aquatic Ecosystem Stress and Recovery, 6 (1997) 43-55.
[52] F. Haider, E.P. Sokolov, I.M. Sokolova, Effects of mechanical disturbance and salinity stress on bioenergetics and burrowing behavior of the soft-shell clam *Mya arenaria*, Journal of Experimental Biology, 221 (2018).
[53] M.W. Pfaffl, A new mathematical model for relative quantification in real-time RT-PCR, Nucleic Acids Research, 29 (2001) 2002-2007.
[54] B. Sanni, K. Williams, E.P. Sokolov, I.M. Sokolova, Effects of acclimation temperature and cadmium exposure on mitochondrial aconitase and LON protease from a model marine ectotherm, *Crassostrea virginica*, Comparative Biochemistry and Physiology, Part C, 147 (2008) 101-112.
[55] B. Marchi, B. Burlando, M.N. Moore, A. Viarengo, Mercury- and copper-induced lysosomal membrane destabilisation depends on $[Ca^{2+}]_i$ dependent phospholipase A2 activation, Aquatic Toxicology, 66 (2004) 197-204.
[56] S. Devin, T. Burgeot, L. Giambérini, L. Minguez, S. Pain-Devin, The integrated biomarker response revisited: optimization to avoid misuse, Environ. Sci. Pollut. Res., 21 (2014) 2448-2454.

[57] I.M. Sokolova, M. Frederich, R. Bagwe, G. Lannig, A.A. Sukhotin, Energy homeostasis as an integrative tool for assessing limits of environmental stress tolerance in aquatic invertebrates, Marine Environmental Research, 79 (2012) 1-15.
[58] P. Calow, Proximate and ultimate responses to stress in biological systems, Biological Journal of Linnean Society, 37 (1989) 173-181.
[59] M.R. Berenbaum, A.R. Zangerl, Costs of Inducible Defense: Protein Limitation, Growth, and Detoxification in Parsnip Webworms, Ecology, 75 (1994) 2311-2317.
[60] H. Attia, H. Nounou, M. Shalaby, Zinc Oxide Nanoparticles Induced Oxidative DNA Damage, Inflammation and Apoptosis in Rat's Brain after Oral Exposure, Toxics, 6 (2018) 29.
[61] S. Ansar, M. Abudawood, S.S. Hamed, M.M. Aleem, Exposure to Zinc Oxide Nanoparticles Induces Neurotoxicity and Proinflammatory Response: Amelioration by Hesperidin, Biol Trace Elem Res, 175 (2017) 360-366.
[62] H. Wang, J. Ye, Regulation of energy balance by inflammation: common theme in physiology and pathology, Reviews in endocrine & metabolic disorders, 16 (2015) 47-54.
[63] G. Lannig, J.F. Flores, I.M. Sokolova, Temperature-dependent stress response in oysters, *Crassostrea virginica*: Pollution reduces temperature tolerance in oysters, Aquatic Toxicology, 79 (2006) 278-287.
[64] Y.-S. Lin, S.-C. Tsai, H.-C. Lin, C.-D. Hsiao, S.M. Wu, Changes of glycogen metabolism in the gills and hepatic tissue of tilapia (Oreochromis mossambicus) during short-term Cd exposure, Comparative Biochemistry and Physiology Part C: Toxicology & Pharmacology, 154 (2011) 296-304.
[65] M. Ansaldo, D.E. Nahabedian, E. Holmes-Brown, M. Agote, C.V. Ansay, N.R.V. Guerrero, E.A. Wider, Potential use of glycogen level as biomarker of chemical stress in *Biomphalaria glabrata*, Toxicology, 224 (2006) 119-127.
[66] G. De Boeck, R. Smolders, R. Blust, Copper toxicity in gibel carp *Carassius auratus gibelio*: Importance of sodium and glycogen, Comparative Biochemistry and Physiology Part C: Toxicology & Pharmacology, 152 (2010) 332-337.
[67] A.V. Hallare, M. Schirling, T. Luckenbach, H.R. Kohler, R. Triebskorn, Combined effects of temperature and cadmium on developmental parameters and biomarker responses in zebrafish (*Danio rerio*) embryos, Journal of Thermal Biology, 30 (2005) 7-17.
[68] C. Filippi, A. Pryde, P. Cowan, T. Lee, P. Hayes, K. Donaldson, J. Plevris, V. Stone, Toxicology of ZnO and TiO2 nanoparticles on hepatocytes: impact on metabolism and bioenergetics, Nanotoxicology, 9 (2015) 126-134.
[69] U. Kadiyala, E.S. Turali-Emre, J.H. Bahng, N.A. Kotov, J.S. VanEpps, Unexpected insights into antibacterial activity of zinc oxide nanoparticles against methicillin resistant Staphylococcus aureus (MRSA), Nanoscale, 10 (2018) 4927-4939.
[70] W. Bursch, A. Karwan, M. Mayer, J. Dornetshuber, U. Frohwein, R. Schulte-Hermann, B. Fazi, F. Di Sano, L. Peredda, M. Piacentini, G. Petrovski, L. Fesus, C. Gerner, Cell death and autophagy: Cytokines, drugs, and nutritional factors, Toxicology, 254 (2008) 147-157.
[71] F. Haider, E.P. Sokolov, I.M. Sokolova, Effects of mechanical disturbance and salinity stress on bioenergetics and burrowing behavior of the soft shell clam Mya arenaria, The Journal of Experimental Biology, 221 (2018) jeb.172643-jeb.172643.
[72] A.V. Ivanina, I.M. Sokolova, Interactive effects of pH and metals on mitochondrial functions of intertidal bivalves Crassostrea virginica and Mercenaria mercenaria, Aquatic Toxicology, 144-145 (2013) 303-309.
[73] A.V. Ivanina, I.O. Kurochkin, L. Leamy, I.M. Sokolova, Effects of temperature and cadmium exposure on the mitochondria of oysters (*Crassostrea virginica*) exposed to hypoxia and subsequent reoxygenation, The Journal of Experimental Biology, 215 (2012) 3142-3154.

[74] I.O. Kurochkin, M. Etzkorn, D. Buchwalter, L. Leamy, I.M. Sokolova, Top-down control analysis of the cadmium effects on molluscan mitochondria and the mechanisms of cadmium-induced mitochondrial dysfunction, American Journal of Physiology - Regulatory, Integrative and Comparative Physiology, 300 (2011) R21-R31.
[75] A.V. Ivanina, E. Habinck, I.M. Sokolova, Differential sensitivity to cadmium of key mitochondrial enzymes in the eastern oyster, *Crassostrea virginica* Gmelin (Bivalvia: Ostreidae), Comparative Biochemistry and Physiology Part C: Toxicology & Pharmacology, 148 (2008) 72-79.
[76] A.S. Cherkasov, C. Taylor, I.M. Sokolova, Seasonal variation in mitochondrial responses to cadmium and temperature in eastern oysters *Crassostrea virginica* (Gmelin) from different latitudes, Aquatic Toxicology, 97 (2010) 68-78.
[77] R. Trevisana, G. Delapedra, D.F. Mello, M. Arl, É.C. Schmidt, F. Meder, M. Monopoli, E. Cargnin-Ferreira, Z.L. Bouzon, A.S. Fisher, D. Sheehan, A.L. Dafr, Gills are an initial target of zinc oxide nanoparticles in oysters *Crassostrea gigas,* leading to mitochondrial disruption and oxidative stress, Aquatic Toxicology, (2014).
[78] E.P. Sokolov, I.M. Sokolova, Compatible osmolytes modulate mitochondrial function in a marine osmoconformer Crassostrea gigas (Thunberg, 1793), Mitochondrion, 45 (2019) 29-37.
[79] P.I. Oteiza, Zinc and the modulation of redox homeostasis, Free radical biology & medicine, 53 (2012) 1748-1759.
[80] I. Marisa, V. Matozzo, M. Munari, A. Binelli, M. Parolini, A. Martucci, E. Franceschinis, N. Brianese, M.G. Marin, In vivo exposure of the marine clam Ruditapes philippinarum to zinc oxide nanoparticles: responses in gills, digestive gland and haemolymph, Environmental science and pollution research international, 23 (2016) 15275-15293.
[81] T.M. Bray, W.J. Bettger, The physiological role of zinc as an antioxidant, Free Radical Biology and Medicine, 8 (1990) 281-291.
[82] C.D. Klaassen, J. Liu, B.A. Diwan, Metallothionein protection of cadmium toxicity, Toxicology and Applied Pharmacology, 238 (2009) 215-220.
[83] M.J. Jenny, A.H. Ringwood, K. Schey, G.W. Warr, R.W. Chapman, Diversity of metallothioneins in the American oyster, *Crassostrea virginica*, revealed by transcriptomic and proteomic approaches, European Journal of Biochemistry, 271 (2004) 1702-1712.
[84] X. Yin, S. Zhou, Y. Zheng, Y. Tan, M. Kong, B. Wang, W. Feng, P.N. Epstein, J. Cai, L. Cai, Metallothionein as a compensatory component prevents intermittent hypoxia-induced cardiomyopathy in mice, Toxicology and Applied Pharmacology, 277 (2014) 58-66.
[85] S.R. Davis, R.J. Cousins, Metallothionein Expression in Animals: A Physiological Perspective on Function, The Journal of nutrition, 130 (2000) 1085-1088.
[86] M. Nigro, A. Falleni, I.D. Barga, V. Scarcelli, P. Lucchesi, F. Regoli, G. Frenzilli, Cellular biomarkers for monitoring estuarine environments: Transplanted versus native mussels, Aquatic Toxicology, 77 (2006) 339-347.
[87] M.N. Moore, J. Icarus Allen, A. McVeigh, Environmental prognostics: An integrated model supporting lysosomal stress responses as predictive biomarkers of animal health status, Marine Environmental Research, 61 (2006) 278-304.
[88] P.K. Mandal, A. Mandal, G.A. Ahearn, Zn transport by lobster hepatopancreatic lysosomal membrane vesicles, Journal of Experimental Zoology Part A: Comparative Experimental Biology, 305A (2006) 203-214.
[89] G.A. Ahearn, P.K. Mandal, A. Mandal, Mechanisms of heavy-metal sequestration and detoxification in crustaceans: a review, J Comp Physiol B, 174 (2004) 439-452.

[90] F. Gagné, J. Auclair, S. Trépanier, P. Turcotte, M. Pilote, C. Gagnon, The impact of zinc oxide nanoparticles in freshwater mussels exposed to municipal effluents, Invertebrate Survival Journal; Vol 13 No 1 (2016), (2016).
[91] J. Letendre, F. Leboulenger, F. Durand, Oxidative Challenge and Redox Sensing in Mollusks: Effects of Natural and Anthropic Stressors, in: Oxidative Stress in Vertebrates and Invertebrates (eds T. Farooqui and A. A. Farooqui). Wiley, 2011.
[92] J. Shim, Drosophila blood as a model system for stress sensing mechanisms, BMB reports, 48 (2015) 223-228.
[93] H.-M. Ni, J.A. Williams, W.-X. Ding, Mitochondrial dynamics and mitochondrial quality control, Redox Biology, 4 (2015) 6-13.
[94] L.L. Fava, F.J. Bock, S. Geley, A. Villunger, Caspase-2 at a glance, Journal of Cell Science, 125 (2012) 5911-5915.
[95] M. Lopez-Cruzan, R. Sharma, M. Tiwari, S. Karbach, D. Holstein, C.R. Martin, J.D. Lechleiter, B. Herman, Caspase-2 resides in the mitochondria and mediates apoptosis directly from the mitochondrial compartment, Cell Death Discovery, 2 (2016) 16005.
[96] M. Movassagh, R.S.Y. Foo, Simplified apoptotic cascades, Heart Failure Reviews, 13 (2008) 111-119.
[97] I.M. Sokolova, Apoptosis in molluscan immune defense. , Invertebrate Survival Journal 6(2009) 49-58.
[98] I.M. Sokolova, S. Evans, F.M. Hughes, Cadmium-induced apoptosis in oyster hemocytes involves disturbance of cellular energy balance but no mitochondrial permeability transition, Journal of Experimental Biology, 207 (2004) 3369-3380.
[99] K. Terahara, K.G. Takahashi, Mechanisms and Immunological Roles of Apoptosis in Molluscs, Current Pharmaceutical Design,, 14 (2008) 131*137.
[100] K. Vermeulen, D. Van Bockstaele, Z. Berneman, Apoptosis: mechanisms and relevance in cancer, Ann Hematol, 84 (2005) 627-639.
[101] F. Wang, Z. Yu, W. Wang, Y. Li, G. Lu, C. Qu, H. Wang, M. Lu, L. Wang, L. Song, A novel caspase-associated recruitment domain (CARD) containing protein (CgCARDCP-1) involved in LPS recognition and NF-κB activation in oyster (Crassostrea gigas), Fish & Shellfish Immunology, 79 (2018) 120-129.
[102] C. Freudlsperger, Y. Bian, S. Contag Wise, J. Burnett, J. Coupar, X. Yang, Z. Chen, C. Van Waes, TGF-β and NF-κB signal pathway cross-talk is mediated through TAK1 and SMAD7 in a subset of head and neck cancers, Oncogene, 32 (2012) 1549.
[103] B.R.B. Pires, R.C.M.C. Silva, G.M. Ferreira, E. Abdelhay, NF-kappaB: Two Sides of the Same Coin, Genes, 9 (2018) 24.
[104] L.A. Solt, M.J. May, The IkappaB kinase complex: master regulator of NF-kappaB signaling, Immunologic research, 42 (2008) 3-18.
[105] S. Alexandre, C. Rast, G. Nguyen-Ba, P. Vasseur, ZnCl*2* prevents c-myc repression and apoptosis in serum-deprived Syrian hamster embryo cells, Environmental Toxicology and Pharmacology, 11 (2002) 191-196.
[106] F. Chai, A.Q. Truong-Tran, A. Evdokiou, G.P. Young, P.D. Zalewski, Intracellular zinc depletion induces caspase activation and p21 Waf1/Cip1 cleavage in human epithelial cell lines, The Journal of infectious diseases, 182 (2000) 85-92.
[107] D.K. Perry, M.J. Smyth, H.R. Stennicke, G.S. Salvesen, P. Duriez, G.G. Poirier, Y.A. Hannun, Zinc Is a Potent Inhibitor of the Apoptotic Protease, Caspase-3, Journal of Biological Chemistry, 272 (1997) 18530-18533.
[108] M.J. McCabe, Jr., S.A. Jiang, S. Orrenius, Chelation of intracellular zinc triggers apoptosis in mature thymocytes, Laboratory Investigation [LAB. INVEST.], 69 (1993) 101-110.
[109] A. Albanese, P.S. Tang, W.C. Chan, The effect of nanoparticle size, shape, and surface chemistry on biological systems, Annual review of biomedical engineering, 14 (2012) 1-16.

Supplementary Materials

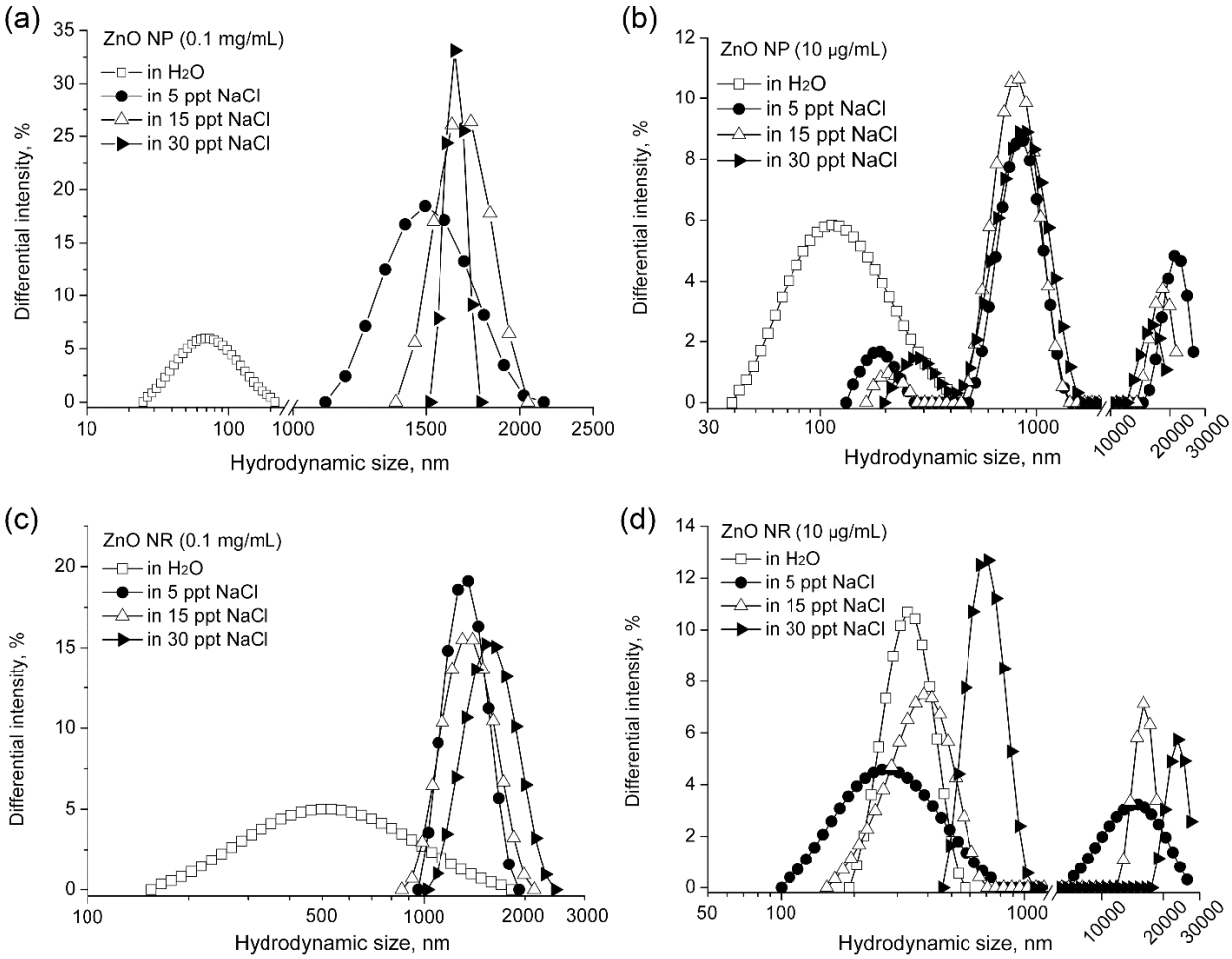

Supplementary Figure 1. Intensity-weighted particle size distribution of (a) ZnO nanoparticles at 0.1 mg/mL, (b) ZnO nanoparticles at 10 µg/mL, (c) ZnO nanorods at 0.1 mg/mL, and (d) ZnO nanorods at 10 µg/mL dispersed in distilled water (H_2O) or in the water of salinity 5, 15 and 30 practical salinity units, respectively.

Supplementary Table 1. Principal component analysis of biomarker responses to nano-ZnO and ionic Zn exposures in *M. edulis*.

Biomarker abbreviations: Cas2 – caspase 2; Cas3 – caspase 3; Cas8 – caspase 8; Bcl2 - B-cell lymphoma 2; Bax - Bcl-2-associated X protein; TGFk - TGF-β-activated kinase 1; NFKb – nuclear factor κB a; IhnNFK1a - inhibitor of NF-κB kinase-1; IhnNFK1b - inhibitor of NF-κB kinase-2; ETS – electron transport system activity; Non-mito – activity of non-mitochondrial reductases; Prot – body protein content; CarbH - body carbohydrates content; Lip - body lipid content; ER – total energy reserves; CEA – cellular energy allocation; MTs – metallothioneins; NRR – neutral red retention time; PC – protein carbonyls; TBARS- thiobarbituric acid-reactive substances; CathDt and CathDf – total and free cathepsin D activity, respectively.

	Principal Components Analysis Eigenvalues. Number of components is 3 Principal Components Analysis sum of variance 30,0000			
Component	Eigenvalues	% Total variance	Cumulative eigenvalue	Cumulative %
1	6,116465	20,38822	6,11647	20,38822
2	4,990258	16,63419	11,10672	37,02241
3	3,765394	12,55131	14,87212	49,57372

	Loading spreadsheet				
Variable	Variable number	Category value	Component 1	Component 2	Component 3
TBARS	2		0,367303	0,623648	0,300342
MTs	3		-0,294226	0,270739	0,149295
CathDt	4		0,314976	0,769176	0,008688
CathDf	5		0,561649	0,686669	0,119032
PC	6		-0,211460	0,421792	0,297889
NRR	7		-0,132901	-0,661692	-0,383504
Cas2	8		-0,590751	0,248685	-0,464973
Cas3	9		-0,724589	-0,083711	0,471711
Cas8	10		-0,724589	-0,083711	0,471711
TGFk	11		-0,571779	0,648237	-0,337072
NFKb	12		-0,540596	0,580234	-0,416316
Bcl2	13		-0,501359	0,687224	-0,283519
Bax	14		-0,354903	-0,029356	0,116629
InhNFK1a	15		-0,292018	-0,111404	-0,163474
InhNFK1b	16		-0,379237	-0,313635	0,658274

CarbH	17		0,092935	0,361900	0,682942
Prot	18		-0,173060	0,028594	0,653968
Lip	19		-0,201826	-0,369855	-0,325166
ER	20		-0,191092	-0,199263	0,105943
Non-Mito	21		-0,848049	0,197582	0,102823
ETS	22		0,729418	0,146755	0,066035
CEA	23		-0,631071	-0,003615	0,008859
Group C	1	109	0,179702	-0,550749	-0,240506
Group NPL	1	110	0,439809	0,438222	0,127950
Group NPH	1	111	-0,727237	0,172830	0,083408
Group NRL	1	112	-0,237696	-0,301450	0,565199
Group NRH	1	113	0,183722	0,476765	-0,165810
Group NRA	1	114	-0,284346	0,121082	-0,585886
Group ZnL	1	115	0,260492	0,088022	0,307784
Group ZnH	1	116	0,185554	-0,444722	-0,092140